ELSEVIER

Progress in Quantum Electronics 34 (2010) 47–87

Progress in Quantum Electronics

www.elsevier.com/locate/pquantelec

Review

The use of plasmonics in light beaming and focusing

Byoungho Lee*, Seyoon Kim, Hwi Kim, Yongjun Lim

National Creative Research Center for Active Plasmonics Application Systems, Inter-University Semiconductor Research Center and School of Electrical Engineering, Seoul National University, Gwanak-Gu Gwanakro 599, Seoul 151-744, Republic of Korea

Abstract

This paper reviews the use of plasmonics to shape light spatially in air and to focus surface plasmon polaritons (SPPs) on a metal surface. Methods to transform SPPs into spatially collimated or focused light by using surface gratings attached around a sub-wavelength slit or modulating the phase of the emitted light from multiple slits are discussed. In addition, it is shown that SPPs passing through diffractive slit patterns, a hole array, or an arc-shape slit can be used to generate focal spots on a metal surface. Before discussing those methods, the basics of SPPs are also briefly reviewed, in order to better understand the handling of SPPs.

keywords: Surface plasmon polariton; Beaming; Beam focusing; Diffractive element

Contents

*Corresponding author. Tel.: +82 2 880 7245.
E-mail address: byoungho@snu.ac.kr (B. Lee).

0079-6727/$ - see front matter © 2009 Elsevier Ltd. All rights reserved.
doi:10.1016/j.pquantelec.2009.08.002

1. Introduction

Recently, studies of the surface plasmon polariton (SPP), which is the coupled mode of an electromagnetic wave and free charges on a metal surface, have attracted considerable interest. This is mainly due to the fact that the low-dimensional behavior of SPP represents a possible solution for the practical realization of photonic integrated circuits or high resolution optical applications such as optical lithography, a hyper lens and optical data storage [1–9]. In particular, SPP has become a focus of research interest after the discovery of the extraordinary optical transmission (EOT) phenomenon, since the unique properties of SPPs surpass the conventional diffraction limitations [10–13]. Since then, numerous interesting topics have arisen that are related to plasmonics, such as optical beaming and EOT from a single sub-wavelength metal hole [14–17].

In this paper, we discuss methods for manipulating light in air or on a metallic surface via the use of SPP. To be specific, the generation of a collimated beam or a focused beam by controlling the radiation properties of SPPs excited on a corrugated metal surface is discussed. In addition, a method for focusing SPP itself on a metal surface using diffractive slit patterns, holes, arc-shape slits or diffractive elements will be discussed. The subjects which will be discussed are briefly categorized in Table 1. However, it will be beneficial to

Table 1
Categorized subjects which will be discussed based on their characteristics.

	Methods	Applications
Spatial fields modulation by using SPP	1. Modulating radiation fields from SPPs by using modifield surface gratings 2. Modulating transmitted fields via modified slit arrays	1. Off-axis beaming 2. Beam focusing
Manipulating SPP itself	1. Using diffractive slit patterns 2. Floating dielectric lens 3. Using phase shift by impinging oblique light	1. Plasmonic focusing and lens 2. Plasmonic multiplexer

understand the basic concepts and properties of SPPs before discussing them in detail. Hence, this aspect will be reviewed first.

2. Surface plasmon polaritons on a metal surface

2.1. Surface plasmon polaritons on a thick metal substrate

As mentioned above, SPP is a propagating surface wave excited on a metal surface [18,19]. More specifically, SPP is an electromagnetic surface wave that is collectively coupled with free charges at the boundary between a metal and a dielectric. It refers to a combined excitation made-up of a surface plasmon, which is an electron plasma oscillation on a metal surface, and a photon [20]. This collective relation between conduction charges on a metal surface and an electric field is depicted in Fig. 1. Due to the charge distribution as shown in Fig. 1(a), electric fields have both z- and x-directional components and the magnetic field has y-directional components. This indicates that SPPs can be excited only by TM-polarized (p-polarized) light. Since the SPP is bound to a metal surface, it is an

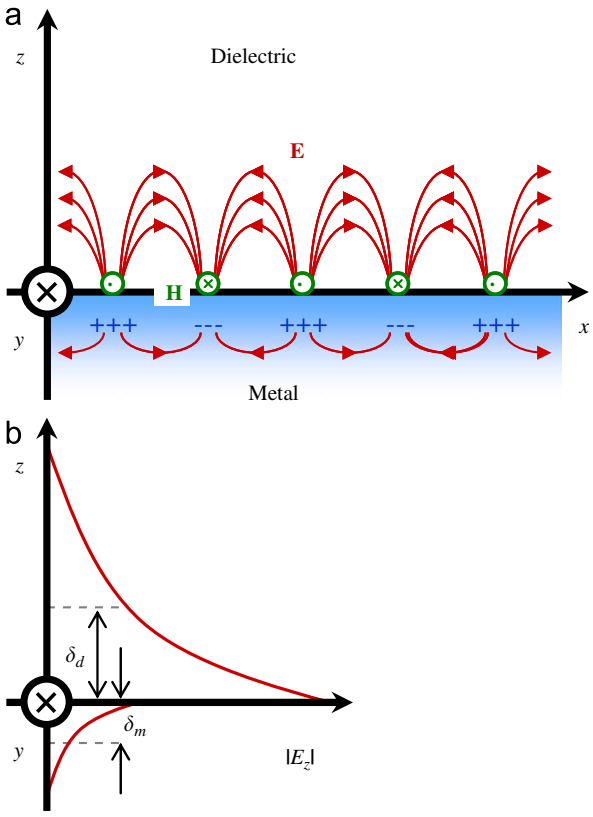

Fig. 1. (a) SPP, which is the collective interaction between free charges on a metal surface and electromagnetic fields and (b) evanescent field of an SPP surface-bound wave.

evanescent field in the z-direction, as shown in Fig. 1(b), and its skin depths into the dielectric and metal are denoted by δ_d and δ_m, respectively.

In general, an SPP can be characterized by the characteristic equation for a stratified metal–dielectric structure or its dispersion relation, and it can be delivered from phase matching condition of Maxwell's equations, as shown in equation below for a single interface structure [18,21–23]:

$$\omega = c_0 k_x \sqrt{\frac{\varepsilon_d + \varepsilon_m}{\varepsilon_d \varepsilon_m}}, \tag{1}$$

where ω is the angular frequency of light or SPP, c_0 the speed of light in vacuum, k_x the propagation constant of SPP, and ε_d and ε_m correspond to electric permittivity (dielectric constant) of dielectric and metal, respectively.

In Eq. (1), the dielectric constant of the metal is frequency-dependent, and it can be expressed as Eq. (2) by the free electron model for a metal, or the Drude model, ignoring the oscillation damping of electrons for convenience.

$$\varepsilon_m(\omega) = 1 - \left(\frac{\omega_p}{\omega}\right)^2, \tag{2}$$

where ω_p is the plasma frequency.

Replacing ε_m of Eq. (1) by Eq. (2) with $\varepsilon_d = 1$, we can obtain the SPP dispersion relation between air and the metal as Eq. (3).

$$\omega = \sqrt{\frac{\omega_p^2}{2} + (c_0 k_x)^2 - \left[\frac{\omega_p^4}{4} + (c_0 k_x)^4\right]^{1/2}}. \tag{3}$$

When $c_0 k_x$ is much smaller than ω_p, Eq. (3) yields Eq. (4a), analogous to a dispersion relation in a homogeneous medium. On the contrary, when $c_0 k_x$ is much larger than ω_p, the SPP dispersion relation becomes saturated to $\omega_p/\sqrt{2}$ with an increase in k_x, as Eq. (4b).

$$\omega \approx c_0 k_x \text{ when } c_0 k_x \ll \omega_p, \tag{4a}$$

$$\omega \approx \frac{\omega_p}{\sqrt{2}}\left[1 - \frac{1}{8}\left(\frac{\omega_p}{c_0 k_x}\right)^2\right] \text{ when } c_0 k_x \gg \omega_p. \tag{4b}$$

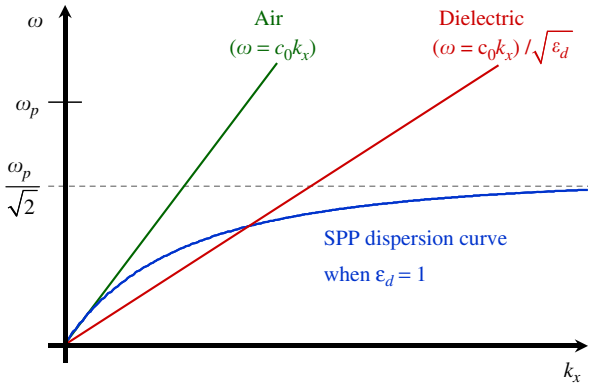

Fig. 2. Dispersion curves for air, dielectric medium ($\varepsilon_d > 1$), and an SPP with an air–metal boundary.

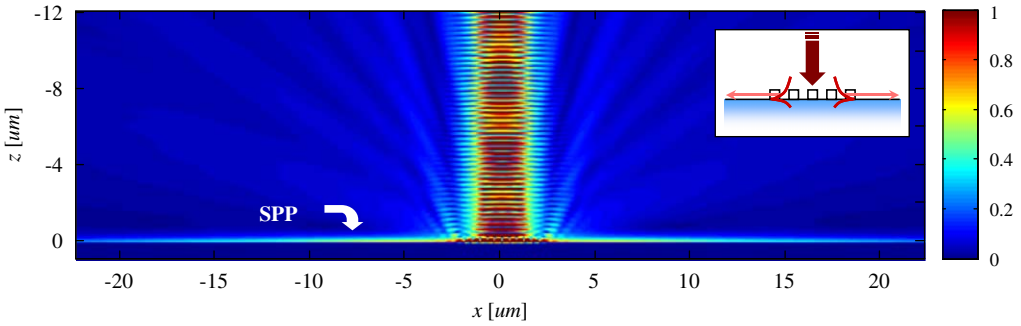

Fig. 3. RCWA simulation result of SPP feature excited by a Gaussian beam on Ag substrate with dielectric surface gratings.

These properties of the SPP dispersion relation are shown in Fig. 2, as well as the dispersion relations of air and a certain dielectric medium [18]. In Fig. 2, the dispersion curves for air and SPP do not meet for any value of k_x except for the origin. This means that it is impossible to match the SPP resonance condition by electromagnetic waves in the air, and the SPP excited on air–metal substrate has a non-radiative property. In other words, for a given ω, the propagation constant k_x of an SPP is larger than wavenumber of light in free space k_0. However, the SPP dispersion curve can have an intersection with a proper dielectric dispersion curve for a given frequency ω. In this respect, similar to the Otto configuration which is one type of attenuated total reflection configurations, dielectric prisms or substrates are generally used to generate an SPP on a metal substrate surface for phase matching. Another method to induce SPP is the use of a grating structure which diffracts incident light to match the resonant conditions, as shown in the inset of Fig. 3. This method is discussed in detail in Chapter 3. Fig. 3 shows a rigorous coupled wave analysis (RCWA) [24–30] simulation result of SPP excited on a metal substrate via the use of a dielectric grating structure on which a Gaussian beam is impinged. Incident source is *p*-polarized 532 nm light, metal substrate is Ag and dielectric surface gratings have refractive index of 1.72, period of 359 nm and fill factor of 0.5.

2.2. Surface plasmon polaritons on a thin metal film

In a way, slightly different from the Otto configuration, an SPP can be excited on a thin metal film even though there is no air gap between the dielectric prism and the thin metal film, as shown in Fig. 4(a). This is referred to as the Kretschmann–Raether configuration, which also has an attenuated total reflection configuration. To demonstrate the existence of SPP, *p*-polarized light is irradiated on 50 nm of Ag film by varying the incidence angle and its reflectance is calculated. The wavelength of light is 532 nm and the refractive index of the dielectric prism is 1.46 in this example. As shown in Fig. 4(b), reflectance plummets at specific angle, about 46.3°, and this phenomenon indicates that the SPP is excited on the thin metal surface for this incidence angle of light. With the observed resonance angle θ_{SPP}, we can know from Eq. (5) that the real part of the excited SPP propagation constant k_{SPP} normalized by k_0 is 1.055, a value that is larger than the wavenumber in free space, k_0.

$$\mathrm{Re}(k_{spp}) = nk_0 \sin\theta_{spp}, \tag{5}$$

where n is the refractive index of the dielectric prism.

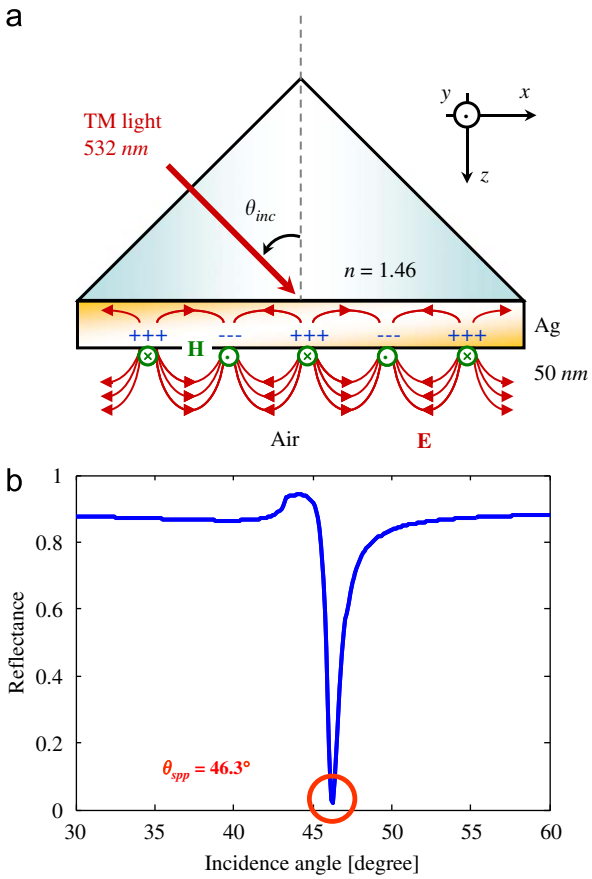

Fig. 4. (a) Kretschmann–Raether configuration for exciting surface plasmon polariton and (b) reflectance by varying the incidence angle.

With this resonance condition, SPPs on a thin metal film excited with a Gaussian beam and a pulsed Gaussian beam are shown in Fig. 5. There are two distinctive features in Fig. 5. First, the excited SPPs are damped as they propagate. This is mainly due to the fact that SPPs undergo Ohmic loss in metal. Second, SPPs emit radiation into the dielectric prism as they propagate, since their propagation constant normalized by k_0, 1.056, enables non-evanescent radiation fields for the refractive index of the dielectric prism. This is the main reason why this SPP is radiative in contrast to an SPP on a metal substrate in Fig. 1(a). This damping mechanism is referred to as damping radiation.

In addition to this radiative SPP, or leaky mode, there is another SPP mode on the thin metal surface, namely, the bound mode. This bound mode cannot be excited by propagating light because its propagation constant is generally larger than nk_0. The characteristic equation of multi-layered metal–dielectric structure of Fig. 4(a), which is shown in Eq. (6), can be used to demonstrate this bound SPP mode. In Eq. (6), subscripts

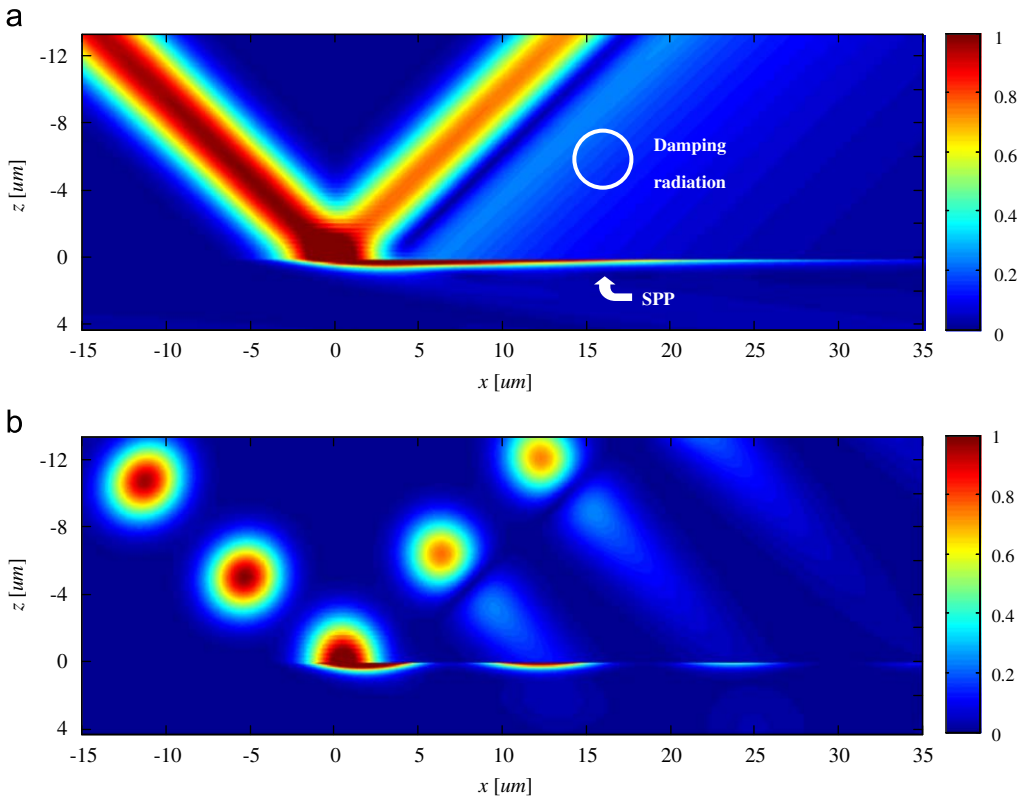

Fig. 5. (a) |**E**| of SPPs on a thin metal film excited by a Gaussian beam and (b) |**E**| of SPPs on a thin metal film excited by a pulsed Gaussian beam. They are simulated by the transfer matrix method.

m, 1, and 2 represent metal layer, input region, and output region, respectively, and d is the thickness of metal film.

$$\left(\frac{\varepsilon_m k_{z,1}}{\varepsilon_1 k_{z,m}}+1\right)\left(\frac{\varepsilon_m k_{z,2}}{\varepsilon_2 k_{z,m}}+1\right)-\left(\frac{\varepsilon_m k_{z,1}}{\varepsilon_1 k_{z,m}}-1\right)\left(\frac{\varepsilon_m k_{z,2}}{\varepsilon_2 k_{z,m}}-1\right)\exp(j2k_{z,m}d)=0. \tag{6}$$

The two propagation constant solutions of characteristic equation mean leaky and bound modes on this structure, and their values are $1.055+j1.097\times10^{-3}$ and $1.658+j2.210\times10^{-2}$ (normalized to k_0), respectively. The first mode, as shown in Fig. 6(a), is the leaky mode which can be excited by a spatially propagating light due to its lower propagation constant and it accompanies damping radiation as it propagates. The second mode, as shown in Fig. 6(b), is the bound mode, and its propagation constant is larger than the wavenumber of light in the dielectric prism. Therefore, it cannot be induced by a propagating light.

As implied in their names, it would be expected that they would be confined to the thin metal film. To be specific, the bound SPP mode is much more confined to the thin metal film than the leaky mode. These properties determine their propagation length which is the

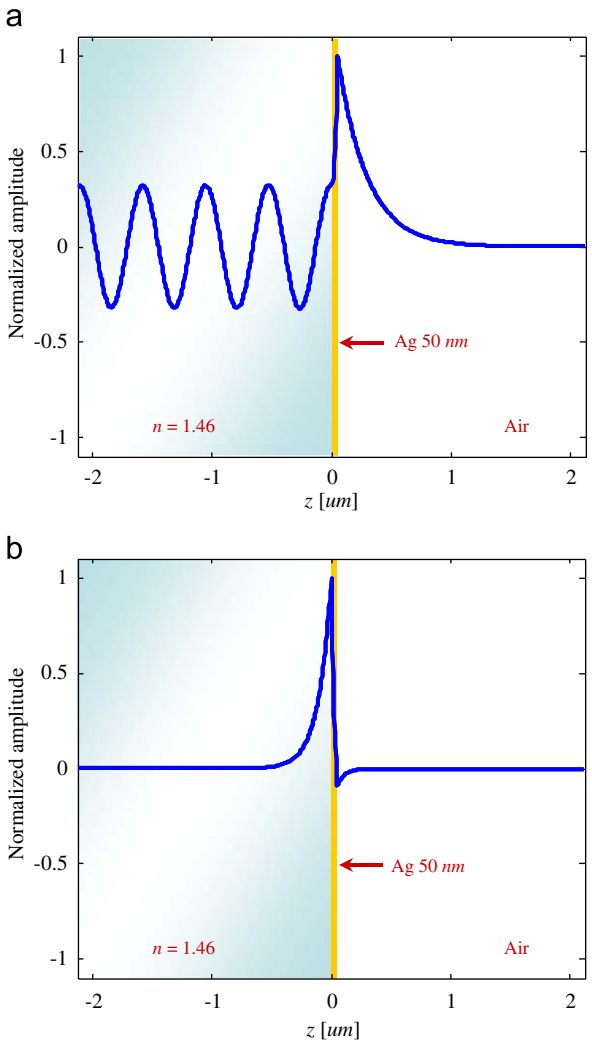

Fig. 6. Amplitudes of **H** of (a) the leaky mode and (b) the bound mode.

length at which the intensity of the SPP is decreased by $1/e$, and it is defined by the imaginary part of the propagation constant k_{spp}, as in Eq. (7).

$$L = \frac{1}{2\,\mathrm{Im}(k_{spp})}. \tag{7}$$

It can be easily calculated from Eq. (7) that the propagation length of the leaky mode is 38.6 μm, which corresponds to 72.5 wavelengths, and that the propagation length of the bound mode is 1.92 μm, which corresponds to 3.60 wavelengths. The main reason for the large difference between the two propagation lengths is due to their confinement degree on the thin metal film. To be specific, in leaky mode, SPPs are confined loosely on metal–dielectric interface, as shown in Fig. 6(a). It means that SPPs undergo less Ohmic

loss as propagating on metal–dielectric interface. In contrast to leaky mode, bound mode SPPs are highly confined on metal–dielectric interface, and hence, the bound mode leads to larger Ohmic loss than leaky mode. As a result, there is significant difference in propagating length between leaky and bound modes.

3. Beam shaping using surface plasmon polaritons excited on a corrugated metal surface

3.1. Surface plasmon polariton on gratings

Before discussing SPPs excited on a corrugated metal surface, two important points related to SPPs excited on a flat surface including metal substrate and a thin metal film are reviewed.

First, in a thin metal film structure with a dielectric prism, it has been shown that the dielectric prism plays a crucial role in matching the resonance condition because the wavenumber in it is larger than k_0, and it can excite the SPP, while the maximum wavenumber of light in free space is just k_0. The portentous aspect of this situation is that a dielectric prism, which is a structure used to excite an SPP, can serve as a passage for the SPP to re-radiate into the outside.

Second, in Fig. 3, the surface gratings on the metal substrate are adopted so as to match the impinging light with the resonance condition. Considering this point, in the first respect, it would be readily expected that these surface gratings on a metal substrate not only act as a passage for impinging light to become an SPP, but also are able to serve as an outlet for an SPP to radiate light. This property is the key concept behind generating collimated beams from sub-wavelength slits or holes surrounded by corrugated surfaces.

In order to demonstrate these properties, we will scrutinize the properties of an SPP excited on a corrugated metal surface with different surface dielectric gratings. These properties are not significantly different when the surface gratings are made-up of metal grooves, and this aspect will be discussed in Section 3.2. There can be three types of surface gratings, referred to as grating types A, B, and C. Their features are depicted in Fig. 7.

SPPs excited on different corrugated surfaces can be explained by the Bloch theorem, or the Floquet condition, as shown in Eq. (8).

$$\mathrm{Re}(k_{spp}) = k_x + m\frac{2\pi}{\Lambda}, \tag{8}$$

where $k_x = k_0 \sin\theta_{inc}$, m is an integer, and Λ the grating period.

In Eq. (8) it can be seen that, even though its left-hand side and k_x are of opposite signs, the equality can be satisfied by adjusting the grating period Λ. For the grating type A, when the incident beam impinges obliquely on the corrugated surface with a negative angle ($\theta_{inc} < 0$) as shown in Fig. 7(a), i.e., $k_x = k_0 \sin\theta_{inc}$ is negative, its-1st-order diffracted wave, which means that $m = 1$ in Eq. (8), excites SPPs propagating along the $+x$-direction. Here, although the diffraction order is -1, m is equal to 1, not -1, because the x-axis component of the incident light wave vector is negative. In contrast to grating type A, SPPs are excited by the 1st-order diffracted wave of incident light in grating type C. This means that incident light having a positive incidence angle ($\theta_{inc} > 0$) excites SPPs propagating along the $+x$-direction for $m = 1$. In grating type B, since SPPs are excited by a perpendicularly incident wave with $k_x = 0$, two SPPs propagating toward the right and left are possible.

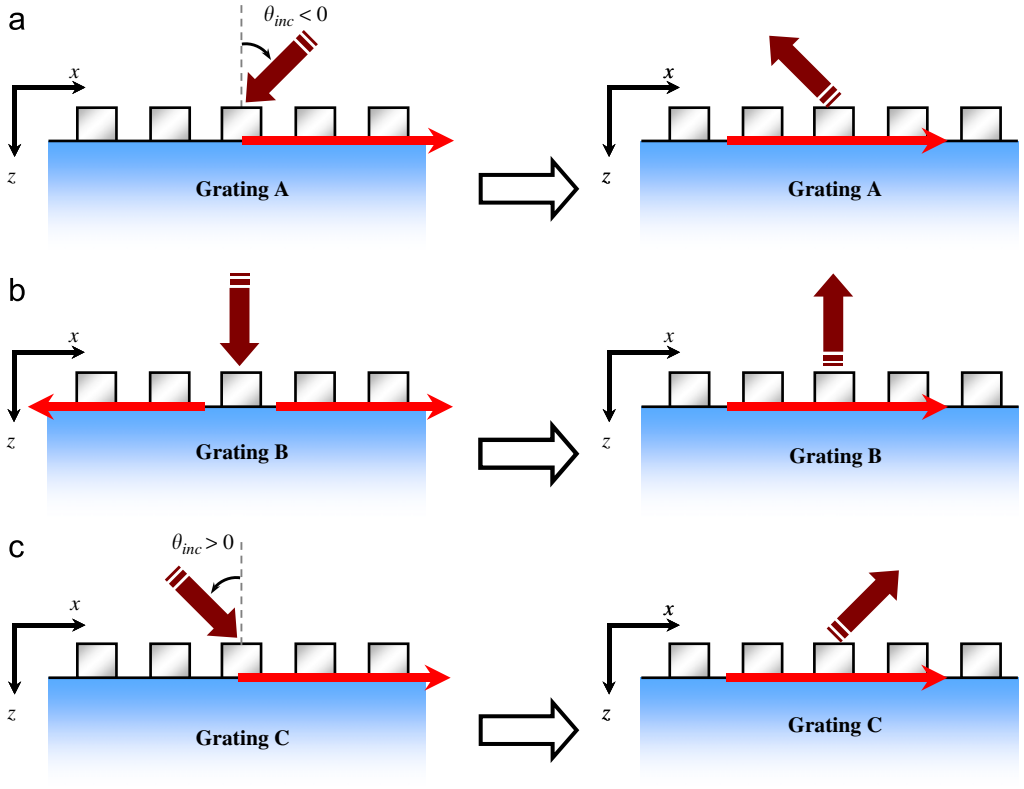

Fig. 7. Three types of dielectric surface gratings showing different radiating properties: (a) grating A showing a backward-coupling property, (b) grating B showing a perpendicular coupling property and (c) grating C showing a forward-coupling property.

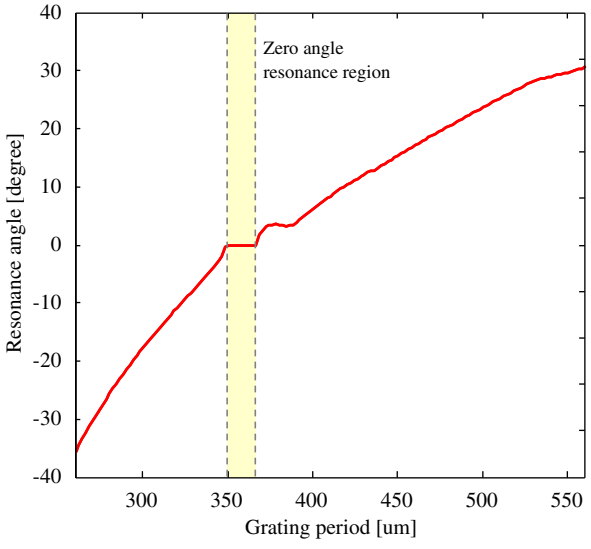

Fig. 8. Resonance angle versus grating period obtained by the numerical analysis using RCWA.

A fine adjustment in designing gratings beyond Eq. (8) can be done by numerical simulation using RCWA, for example. For a fixed grating structure, as varying the incidence angle of *p*-polarized input light, we can figure out the resonance angle that shows the smallest reflectance. Fig. 8 shows the resonance angle versus grating period in which this numerical analysis method was used. Here the input light wavelength is 532 nm, the dielectric gratings have the same refractive index of 1.72, a depth of 100 nm, and a fill factor of 0.5. In addition, the substrate is composed of Ag.

The "−" or "+" sign in resonance angle means the directional coincidence between the incident light and the *x*-axis (or induced SPP) [31–34]. To be specific, the resonance angle has a "+" sign if the *x*-directional component of the incident light wave vector is in the

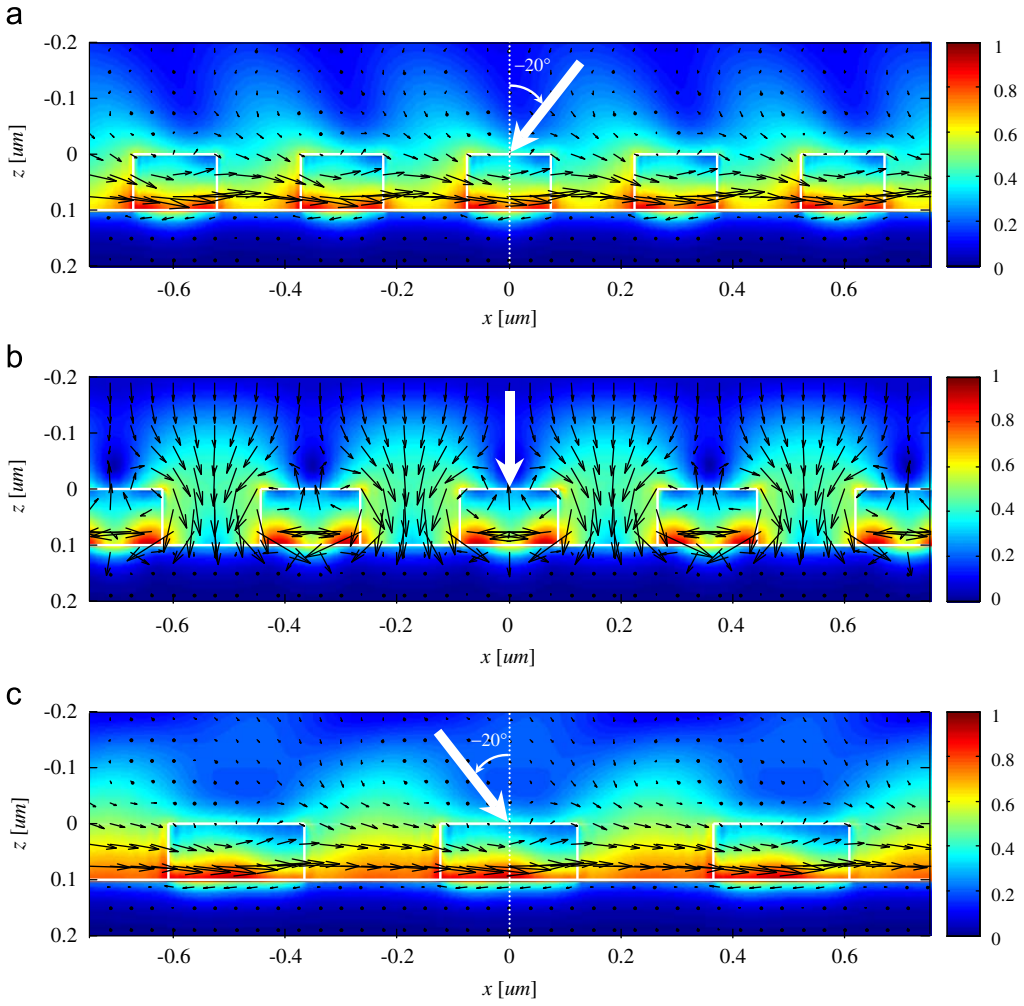

Fig. 9. RCWA simulation results of |**E**| and power flows for *p*-polarized light having wavelength of 532 nm and SPPs induced on a corrugated metal surface, made up of (a) grating A (grating period = 298 nm, resonance angle = −20.0°, $\mathrm{Re}(k_{spp})/k_0 = -1.443$), (b) grating B (359 nm, 0°, ±1.482) and (c) grating C (487 nm, 20.0°, 1.434).

$+x$-direction, analogous to the situation for grating C, where SPP is also propagating in the $+x$-direction. On the contrary, the sign of resonance is "$-$", analogous to the situation for grating A, if the x-directional component of the incident light wave vector is in the $-x$-direction.

Fig. 9 shows a diagram of SPPs excited on a corrugated metal substrate with gratings A, B, and C. The background images show $|\mathbf{E}|$ when lights, having a specific incidence angle, impinge on each corrugated surface, and the black arrows represent the power flow of light and the SPPs in each structure. In grating A, the SPPs are propagating toward the right, while the incident light impinges with a negative incidence angle. In grating C, SPPs excited on the corrugated surface have the same propagation direction as the x-directional component of the incident light wave vector. In grating B of Fig. 9(b), there are two types of SPPs propagating toward left and right because of its symmetrical structure and resonance condition of the perpendicular light.

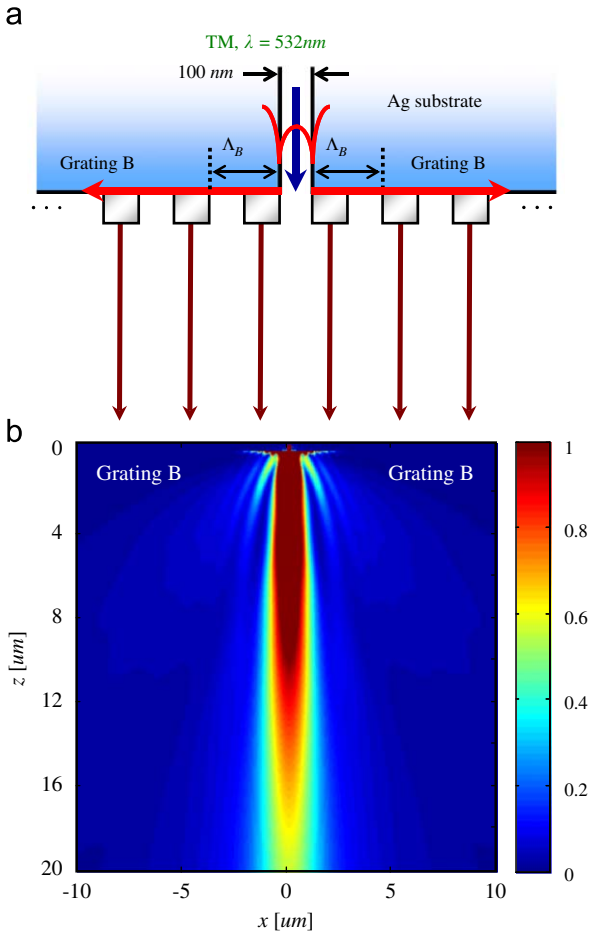

Fig. 10. (a) Basic scheme for generating on-axis beam and (b) RCWA simulation result of on-axis beaming representing intensity distribution.

3.2. On-axis beaming and off-axis beaming

The various gratings described above can generate an on-axis beam, which propagates perpendicularly to the metal surface, and the off-axis beam, which has some deviation angle with respect to the on-axis [31–35].

First, in the case of symmetrically attached gratings of type B around the sub-wavelength metal slit, the SPPs that are exuded from the slit can radiate light in a perpendicular direction as they propagate on the corrugated surface, as shown in Fig. 10. In addition, it is possible to generate an off-axis beam, the angle of which deviates somewhat from the z-direction, by asymmetrically attaching gratings A and C on the metal substrate [34,35]. In this case, SPPs propagating on grating A radiate in the backward off-axis direction. In the case of grating C, excited SPPs radiate in the forward off-axis direction due to their radiation property. Thus, those two different components end up with radiation in the same direction, and they ultimately generate an off-axis beam, as shown in Fig. 11.

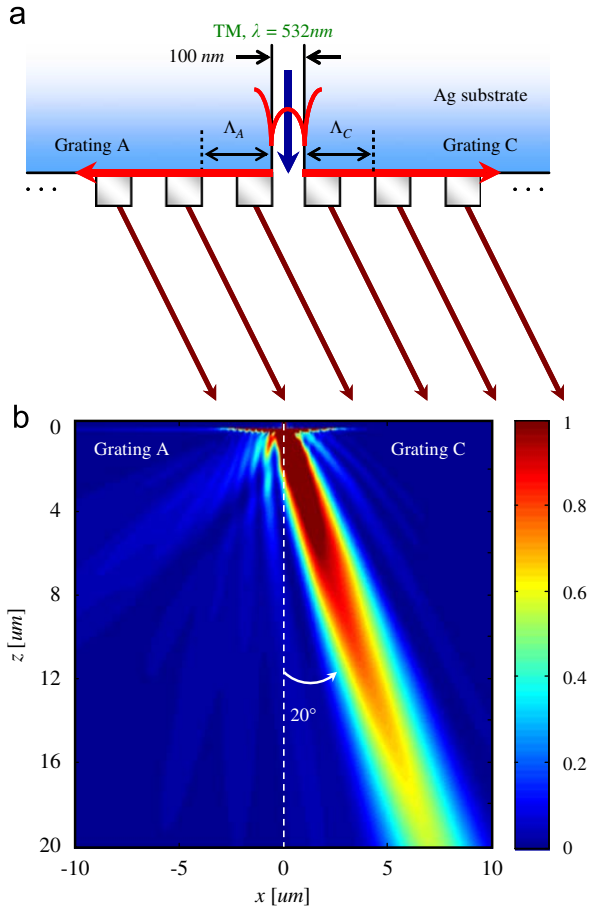

Fig. 11. (a) Basic scheme for generating an off-axis beam and (b) RCWA simulation result of off-axis beaming representing intensity distribution.

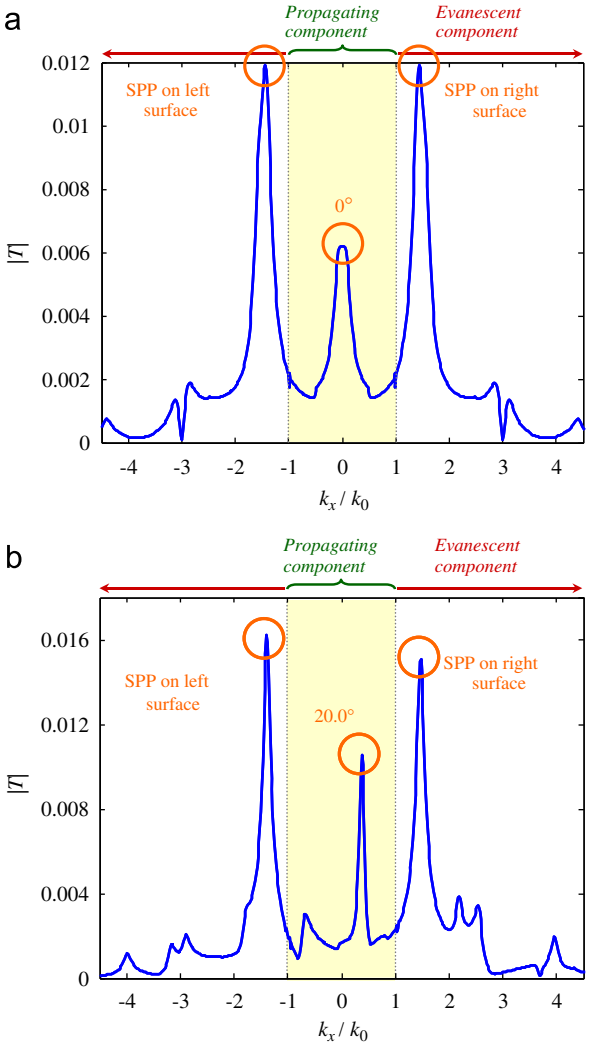

Fig. 12. Angular Fourier spectrum of (a) on-axis beaming, (b) off-axis beaming. $|T|$ denotes the square root of the transmittance at each k_x/k_0.

The properties of on-axis beaming and off-axis beaming are much clearer to comprehend when their angular Fourier spectra are analyzed. In Fig. 12(a), since a collimated beam propagates perpendicularly, the peak is positioned at the center. In addition, in the evanescent component region, there are two symmetric peaks due to SPPs that are induced on the corrugated surface. Similarly, Fig. 12(b) shows the angular Fourier spectrum of off-axis beaming, and a peak appears at 20.0°, representing the off-axis beam. In addition, there are two distinctive peaks in the evanescent component regions. The left peak is the result of SPPs excited on grating A, and the right peak corresponds to an SPP

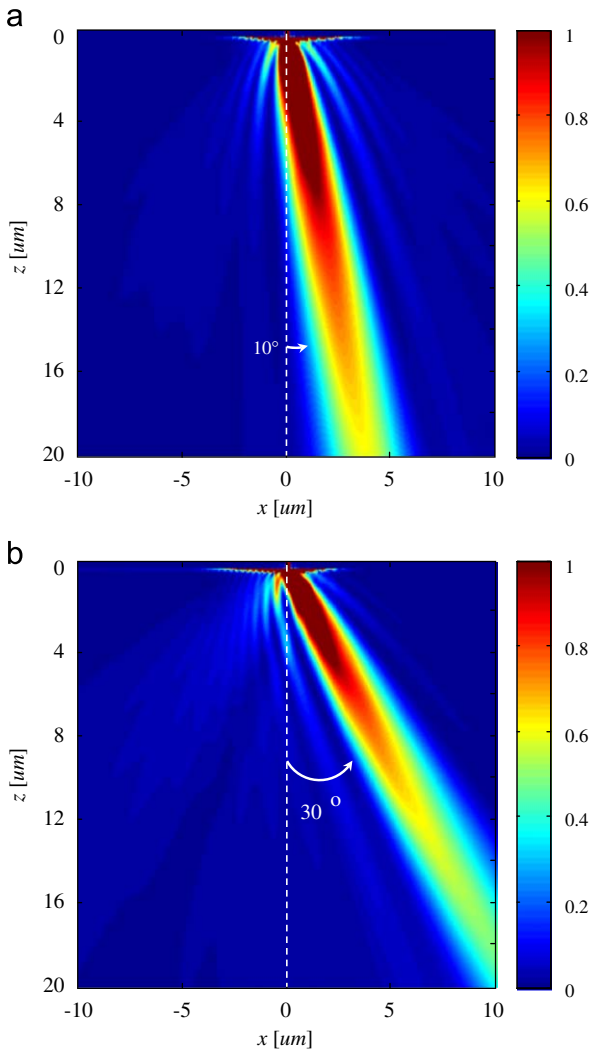

Fig. 13. RCWA simulation results: (a) intensity distribution of an off-axis beam having a deviation angle of -10° and (b) intensity distribution of an off-axis beam having a deviation angle of -30°.

propagating on grating C in Fig. 11(a). This feature has been proved experimentally as shown in Ref. [35], and we will also represent it with beam focusing in Section 4.1.

As can be seen in Fig. 8, it is possible to change the deviation angle of the beam by adjusting the periods of the surface gratings attached to the metal substrate. First, when the period of grating A is 327 nm for a resonance angle of -10° and the period of grating C is 425 nm for a resonant angle of 10°, the coherent deviation angle becomes 10°. In a similar manner, it is possible to change the deviation angle to 30° if the periods of gratings A and C are 274 and 564 nm, respectively. These beams, with different deviation angles are presented in Fig. 13.

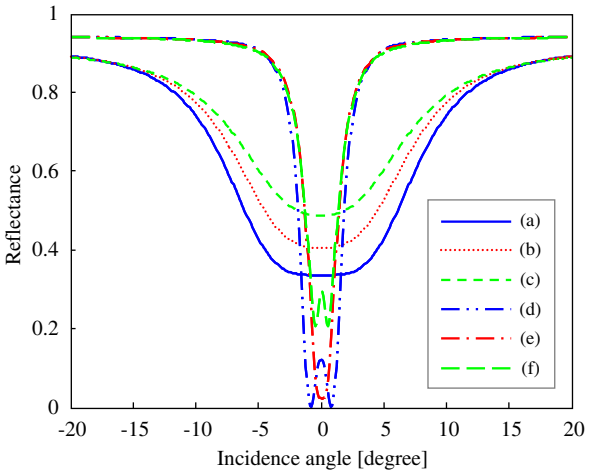

Fig. 14. Reflectance of different gratings as the incidence angle is varied, representing the sensitivity of dielectric surface gratings and metallic grooves. Dielectric gratings have a height of 100 nm and a refractive index of 1.72. Metallic gratings have a height of 25 nm. Each grating has Ag substrate. The grating periods for on-axis radiation are 359 and 492 nm for the dielectric and metallic gratings, respectively. (a) Dielectric grating with period of 354 nm, (b) dielectric grating with period 359 nm, (c) dielectric grating with period of 364 nm, (d) metallic grating with period of 487 nm, (e) metallic grating with period of 492 nm, and (f) metallic grating with period of 497 nm.

The difference between a metallic groove surface and a corrugated surface with dielectric surface gratings is now discussed. It is true that there is little difference between them macroscopically. In other words, it is possible to generate an on-axis beam or an off-axis beam using a metallic groove surface in the same way as discussed above. However, the use of dielectric surface gratings has been shown to be more efficient than the use of a metallic groove surface. This is largely due to the fact that a dielectric is much easier to manufacture than metal. In spite of its ease of processing, dielectric surface gratings also show good marginal tolerance. In addition, as shown in Fig. 14, a metallic grating is very sensitive to its configuration. In this case, slight errors in manufacturing can lead to the distortion in the total field distribution. To be specific, if there is an ± 5 nm error in manufacturing, dielectric surface gratings still have a resonant angle at 0°, although their maximum values and shapes are slightly different. However, in metallic gratings, ± 5 nm errors result in large deviations in the resonant angle. In this sense, a dielectric surface grating is more feasible for practical use than a metallic groove structure.

In fact, those characteristics and sensitivities stem from the exciting features of SPPs. To be specific, on metallic gratings, SPPs propagate along the metallic grating profile, as shown in Fig. 15(a). Therefore, if the profile is shifted slightly, its resonant condition is changed significantly. However, on dielectric surface gratings, SPPs pass through the gratings, as shown in Fig. 15(b), and, as a result, are less sensitive to fabrication errors.

3.3. *Usage of periodic metallic gratings in active elements*

In this section, the use of periodic metallic gratings in active elements to couple more light into nano-photodiode as well as to generate a small divergence beam from semiconductor lasers is discussed.

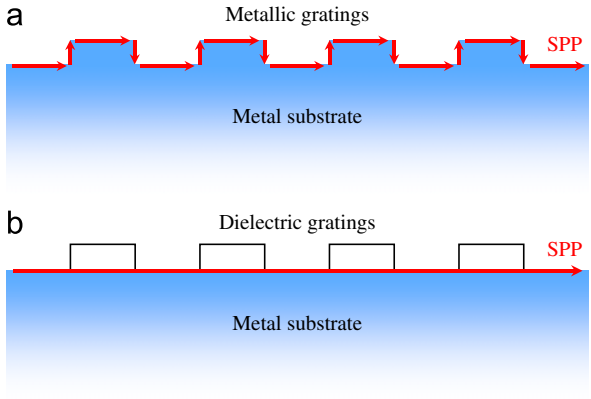

Fig. 15. Propagating features of SPPs (a) on metallic grating, (b) on a dielectric surface grating.

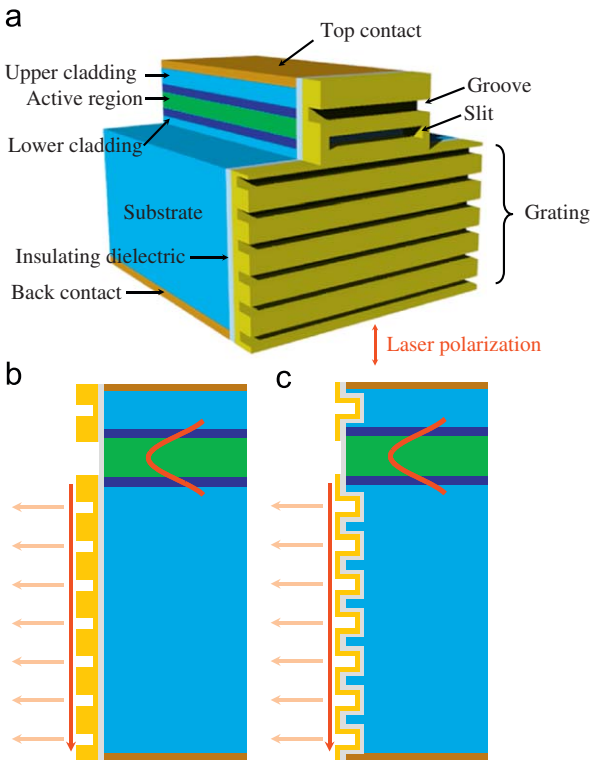

Fig. 16. (a) The basic scheme for a small divergence laser, (b) cross section of metallic groove gratings structure, and (c) cross section of trenched metal-film gratings structure.

First, using those radiating properties of SPPs propagating on a corrugated surface, SPPs have been used in semiconductor lasers [36]. In these lasers, beam divergence, which is an intrinsic problem in the field from an aperture, can be reduced significantly. The basic schemes for these lasers are presented in Fig. 16.

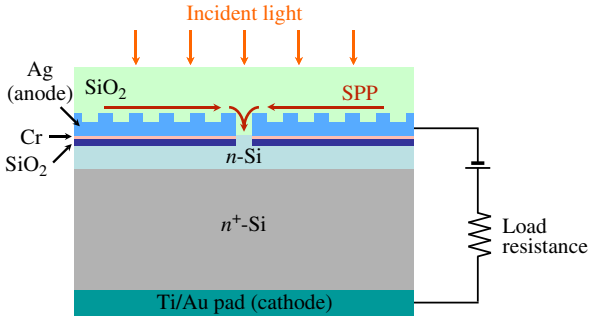

Fig. 17. The basic scheme for a nano-photodiode with metallic grooves inducing surface plasmon polaritons.

The basic process of this small divergence laser is very similar to on-axis beaming. First, an electromagnetic wave emitted from a quantum cascade laser interacts with a metal surface at the outlet, and becomes coupled to SPPs. Second, as these SPPs propagate on the corrugated surface, they end up with coherent radiation, and those radiating fields generate a small, vertical divergence beam with collimated high power. It is also possible to generate not only a vertically collimated but also a laterally collimated beam when a two-dimensional periodic structure is attached to the outlet of the laser [37]. Furthermore, this feature is utilized in plasmonic polarizer which can generate divergence-reduced linearly or circularly polarized light [38].

Secondly, other research has shown that attaching these periodic metallic grooves to the nano-photodiode result in more light being received [39], as shown in Fig. 17. As would be expected, the coupling efficiency of converting incident light into a sub-wavelength metal hole can be increased with the aid of periodic metallic grooves. As a result, the induced current in the photodiode becomes larger with a smaller detector capacitance, suggesting that this structure could be used in a high-speed optical response system. A similar idea was used to devise the concept of wavelength-dependent light sorting [40].

3.4. Beaming in photonic crystals

Up to this point, we have discussed methods for manipulating beams by controlling radiating fields from SPPs propagating on corrugated surfaces. However, there are also interesting methods for manipulating beams that involve the use of photonic crystals although they are not in the fields of plamoncis [41–44], and we will introduce these briefly.

The basic concept of manipulating a beam using a photonic crystal is very similar to that for SPPs. First, light passing through a sub-wavelength photonic crystal waveguide becomes coupled to the corrugated surface of the photonic crystal structure. Second, this coupled light, which corresponds to the evanescent surface mode of the photonic crystal, propagates on the end facets of the photonic crystal structure. In this process, if the termination of the photonic crystal end facets is properly shaped, the surface mode of the evanescent surface waves ends up with coherent radiation, resulting in a highly directional beam with low divergence. In this way, not only it is possible to generate an on-axis

directional beam, but it can also generate an off-axis directional beam by using a surface defect or an asymmetrically arranged surface profile [45,46].

Fig. 18(a) shows a type of beaming structure using photonic crystal waveguide [46]. As mentioned above, the termination of the photonic crystal on the end facets is modulated. In contrast to the fact that the profile of the surface grating is modulated in the beaming structure of the SPP, this structure has index modulated termination. To be specific, as shown in Fig. 18(a), there are cylindrical tubes, which play an important role as defects, consisting of an outer shell with a permittivity of 2.25 and an inner core filled with another material. Therefore, the index profile can be adjusted by changing the material that makes up the inner core. When the cylindrical tubes are filled with dichloroacetic acid ($\varepsilon = 7.8$),

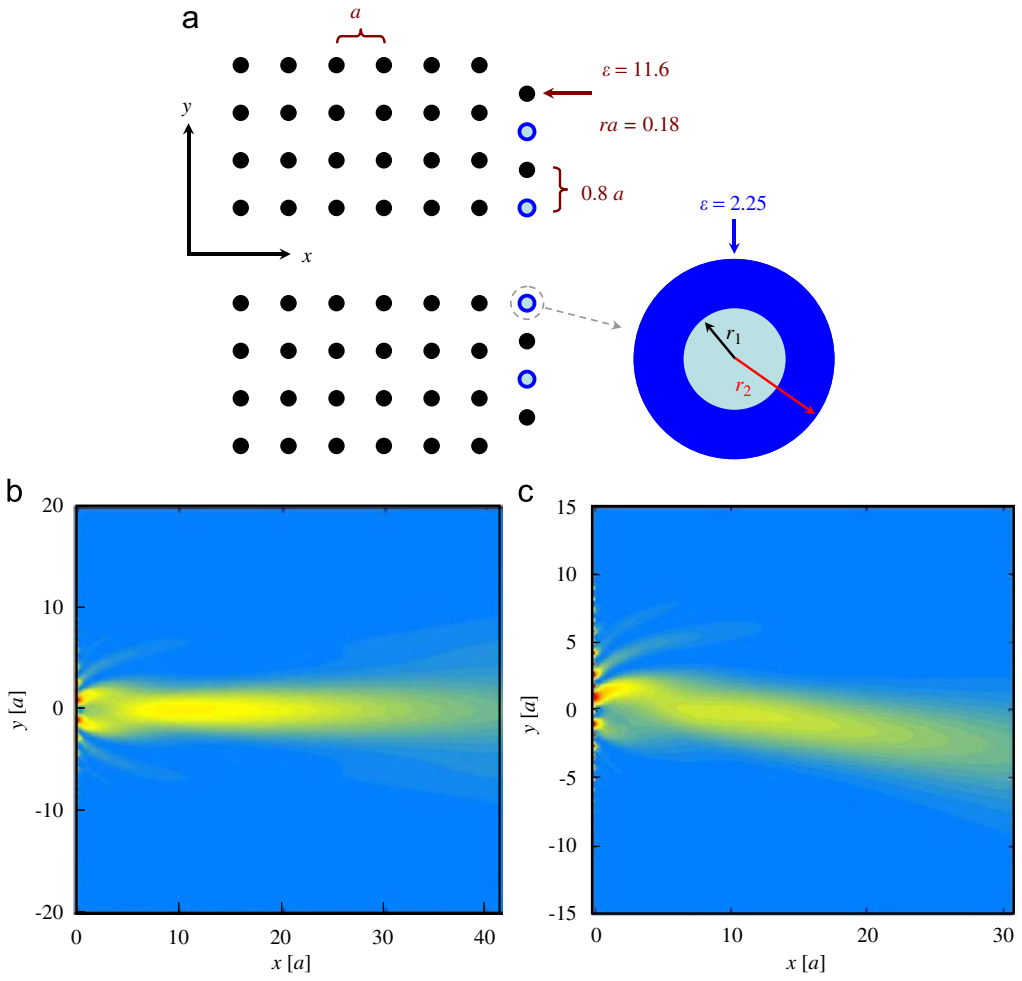

Fig. 18. (a) The basic scheme for a photonic crystal beaming structure, (b) on-axis directional beam emitted from a symmetric index profile termination, (c) off-axis directional beam emitted from an asymmetric index profile termination. (These field distributions of on-axis beaming and off-axis beaming are excerpted from Ref. [46].)

an on-axis directional beam can be produced, as shown in Fig. 18(b) [46]. In a similar manner, it is possible to generate an off-axis directional beam using materials having a permittivity of 9.08 and 6.68, corresponding to methylene chloride and methyl acetate, respectively, as shown in Fig. 18(c) [46].

4. Beam focusing by surface plasmon polaritons

4.1. Beam focusing by using chirped surface gratings

In this Section, methods for focusing light by modulating the radiating fields from surface gratings are discussed. To be specific, the previous surface gratings are modified to produce chirped gratings that produce a focused light pattern [47]. The basic scheme of this focusing structure is shown in Fig. 19.

In this beam focusing structure, we first assume that ray lines, meaning the directions of radiating fields, are emitted from the center of the surface grating height and the boundary between the ridge and the groove of the gratings. Second, a search is made to find the appropriate periods of surface gratings to minimize the error, which is the deviation from the expected focal point at $x = 0$, by trying various surface gratings.

In order to design a beam focusing structure based on the above two criteria, the resonant properties of various surface gratings need to be analyzed, similarly to Fig. 8 (for negative resonance angles). For different resonance angles, $\mathrm{Re}(k_{spp})/k_0$ has slightly different values. Fig. 20 shows an example of numerical simulation in which 12 surface gratings are used to generate a focused beam with a focal length of 1.5 μm. The incident light is *p*-polarized and has a wavelength of 532 nm. The surface gratings have an identical refractive index of 1.72 and height of 120 nm, and their periods are varied from 327.0 to 226.3 nm. The periods of the selected surface gratings decrease gradually with their distance from the slit because the shorter period of a surface grating in a converging region has a larger resonance angle in absolute value. It seems that the beam focusing configuration is similar to that of Fresnel lens or Fresnel zone plate. However, this structure can be discriminated in that it manipulates the side coupling fields, or radiation

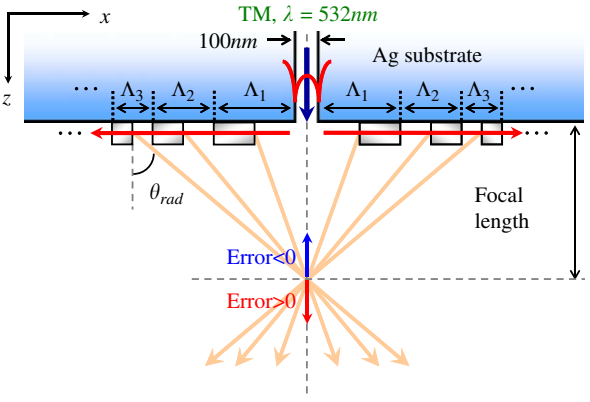

Fig. 19. The basic scheme for a beam focusing structure with chirped surface gratings.

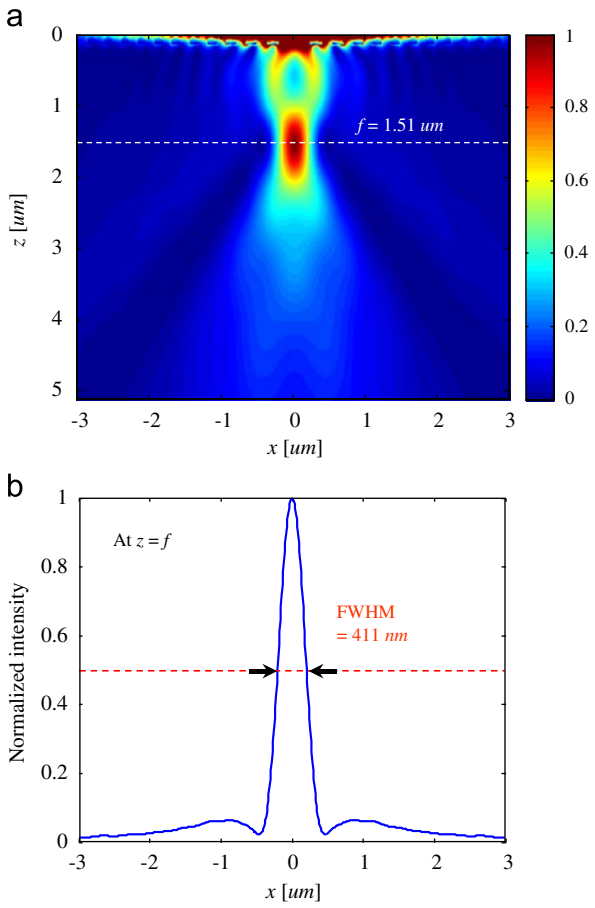

Fig. 20. RCWA simulation results: (a) intensity distribution of a focused beam, formed at 1.51 μm when designed to generate a spot at 1.5 μm and (b) intensity profile at the spot (FWHM: full-width at half-maximum).

fields, into the free space, while the Fresnel lens or the Fresnel zone plate control the fields transmitted through the components.

The intensity distribution of beam focusing when the selected surface gratings are attached around the sub-wavelength slit is shown in Fig. 20(a). The appropriate focal spot is properly formed at 1.51 μm. Moreover, its beam spot is smaller than the wavelength, as shown in Fig. 20(b).

It is also possible to change the position of the focal spot by adjusting the surface gratings. When we design the surface gratings in order to focus light at 2 μm, the focal spot is formed at 1.97 μm and the focal spot is generated at 1.07 μm when we use the surface gratings designed for a focal length of 1 μm [47]. Like this, the beam focusing structure is useful in that it can render focused spot at a few times of wavelength from the substrate easily and accurately, which is difficult to be achieved by the traditional convex lens system. Indeed, the reason why our beam focusing structure has a chirped surface grating profile is that these chirped surface gratings emit a phase modulated field into the air. The concept of phase modulation will be discussed in Section 4.2.

When the number of surface gratings is varied, the width of the beam spot also changes [47]. This phenomenon is mainly due to the Fourier transform relation. To be specific, more radiating elements, which correspond to surface gratings, are necessary for generating a narrower beam spot because of the relation between the field distribution in real space and the spatial frequency domain.

To experimentally test the off-axis plasmonic light beaming and beam focusing, we fabricated those structures. The fabrication recipe refers to the aforementioned design values. Before inscribing the metal slit and the dielectric surface gratings, polymethylmethacrylate (PMMA) with the thickness of 120 nm playing a role as the dielectric layer is spin coated on the Ag layer with the thickness of 300 nm. Both the metal slit and dielectric surface gratings are inscribed by using focused ion beam (FIB) (FEI Corp. Quanta 200 3D) milling. The vertical size of each structure is 9 μm. To detect the light fields of plasmonic light beaming and beam focusing, we constitute a simple microscope adopting a charge coupled device (CCD). Our experimental setup is shown in Fig. 21. In our experimental setup, the second harmonic Nd:YAG laser with the wavelength of 532 nm is used as a light source. Here, to excite the SPP, *p*-polarized light is impinged on fabricated structures. The CCD (Sony Corp.XCD-SX90) with the pixel size of 3.75 μm is used to capture the image, and its resolution is 1280 (horizontal) by 960 (vertical). The object lens with the magnitude of 100 (Olympus Corp. LMPlanFLN) is used as a microscopy, and its numerical aperture is 0.85. According to the focal point of the objective lens, surface images and far-field images can be captured, and they are shown in Fig. 22. In capturing the far-field images, off-axis beaming structure and the beam focusing are respectively 3 and 12 μm away from the surface.

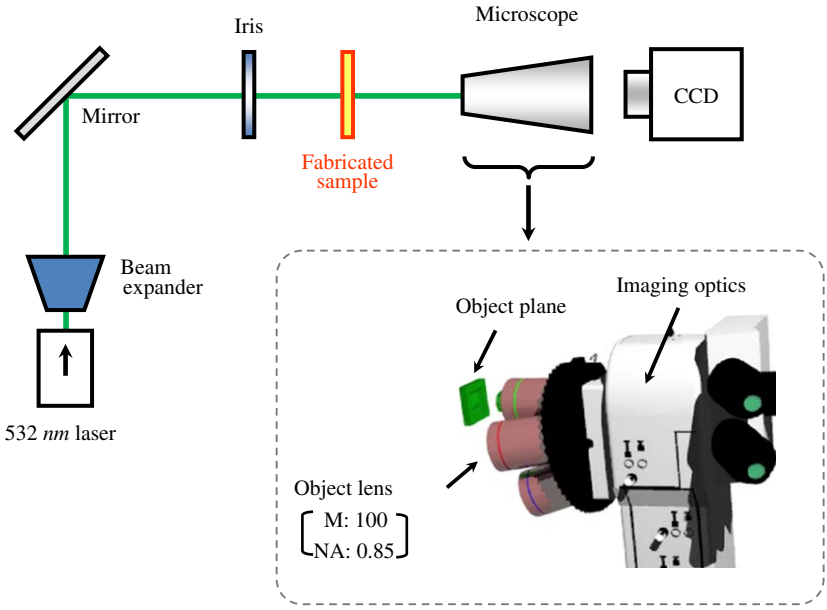

Fig. 21. Experimental setup to capture CCD image of off-axis beaming field and beam focusing field.

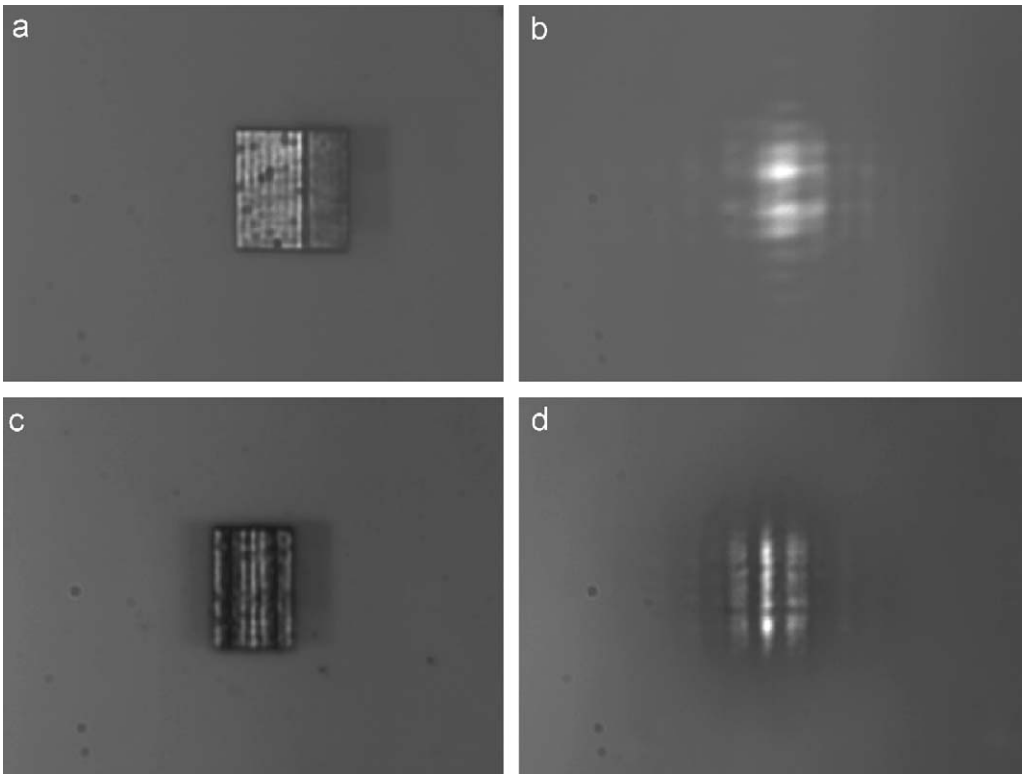

Fig. 22. Captured CCD images: (a) surface image of off-axis beaming, (b) far-field image of off-axis beaming, (c) surface image of beam focusing and (d) far-field image of beam focusing.

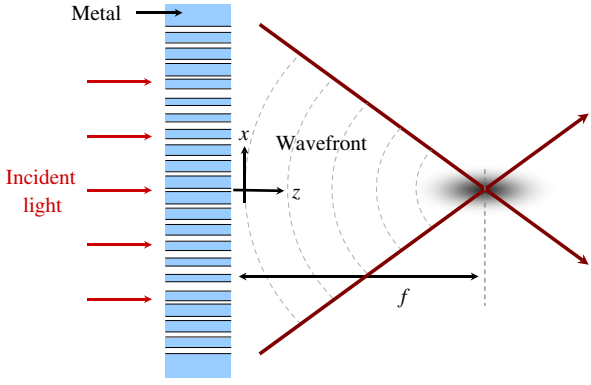

Fig. 23. Beam focusing structure using a nano-slit array with different widths.

4.2. Other beam focusing structures using surface plasmon polaritons

In addition to the use of chirped surface gratings to focus light, there are also a variety of methods available for generating beam spots.

First, there is a method using phase delays of SPPs in different sub-wavelength slits [48]. Since the propagation constant of the slit depends on the width of the slit, SPPs passing through different width sub-wavelength slits experience different retardations. When this property is used appropriately, the phase of the light transmitted through the slit can be controlled in order to generate a desirable phase profile at the exit, as shown in Fig. 23, where Eq. (9) is the phase profile to focus light:

$$\phi(x) = 2n\pi + \frac{2\pi f}{\lambda} - \frac{2\pi\sqrt{f^2 + x^2}}{\lambda}, \tag{9}$$

where f is the focal length and λ the wavelength of the light in free space.

In this structure, if the multiple slits have the same width and are filled with different materials having different permittivities, it is also possible to control phase retardation depending on the materials used. In this sense, the focal spot can be actively controlled by the intensity profile of the incident light when the slits are filled with a nonlinear material because the permittivity of the nonlinear material can be changed by the intensity of the light [49].

Similar to the method in which chirped surface gratings are used, a beam focusing structure can also be produced by modulating the surface gratings [50]. To be specific, this beam focusing structure has a modulated groove depth as shown in Fig. 24. In this case, the relative phase of the light at the center of the groove exit also increases with increasing groove depth, and it varies periodically when the groove depth becomes deeper. As a result, phase modulation can be accomplished by the groove depth profile, similar to a nano-slit array with different widths.

Lastly, it is also possible to produce this phase modulation for beam focusing using plasmonic microzone plates [51,52], as shown in Fig. 25. Basically, this beam focusing structure is based on

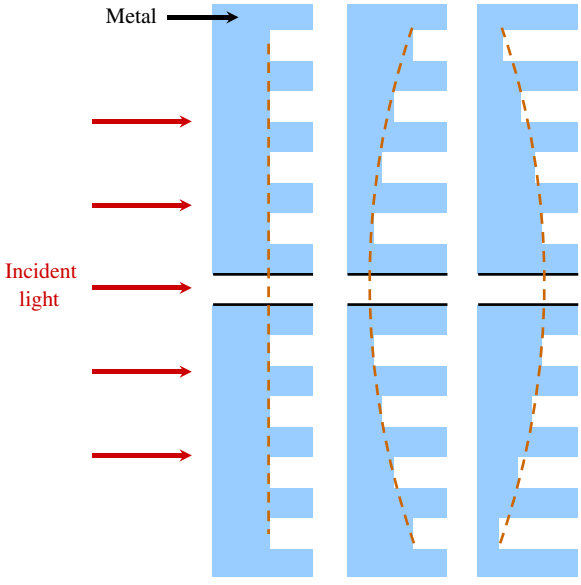

Fig. 24. Different types of modulated groove depth profiles for beam focusing.

the localized SPP wave excited from the slits and the diffraction wave from the zone plate. Although this structure resembles a conventional Fresnel zone plate, its performance in beam focusing exceeds that of a conventional Fresnel zone plate. First, it has powerful focusing performance of elongated focal length and depth of focus with a highly confined spot size beyond the diffraction limit. In spite of such a good performance, its dimension is much smaller than that of a conventional Fresnel zone plate. In addition, the fact that it has a flexible working focal length and relatively small size is useful in terms of practical applications in the fields of optical probes and detection.

5. Focusing surface plasmon polaritons on a metal surface

5.1. Plasmonic focusing by using diffractive slit patterns

As mentioned above, light becomes coupled to SPPs on a metal surface as it passes through perforated holes or slits. In this case, if it is possible to control the coupling

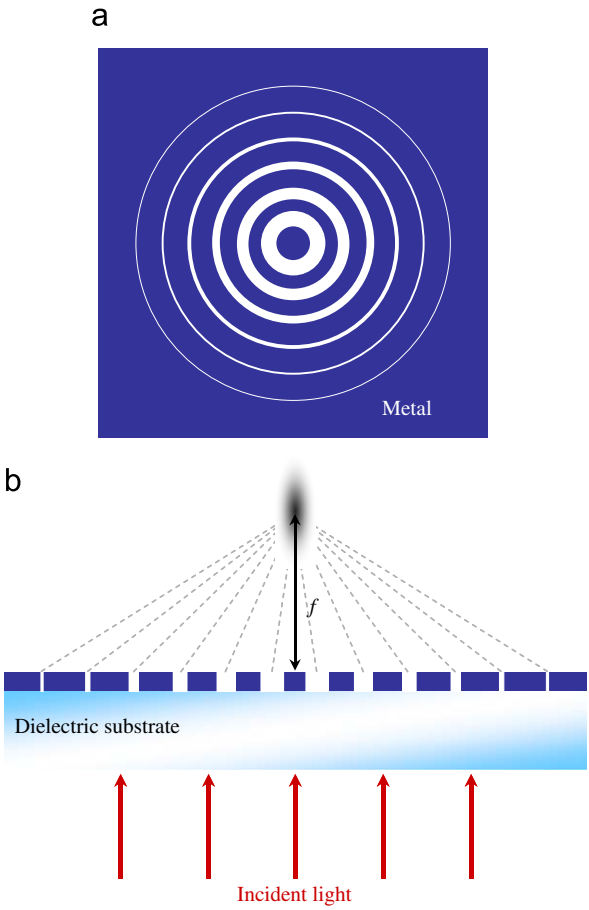

Fig. 25. (a) Top view and (b) cross section of a plasmonic microzone plate.

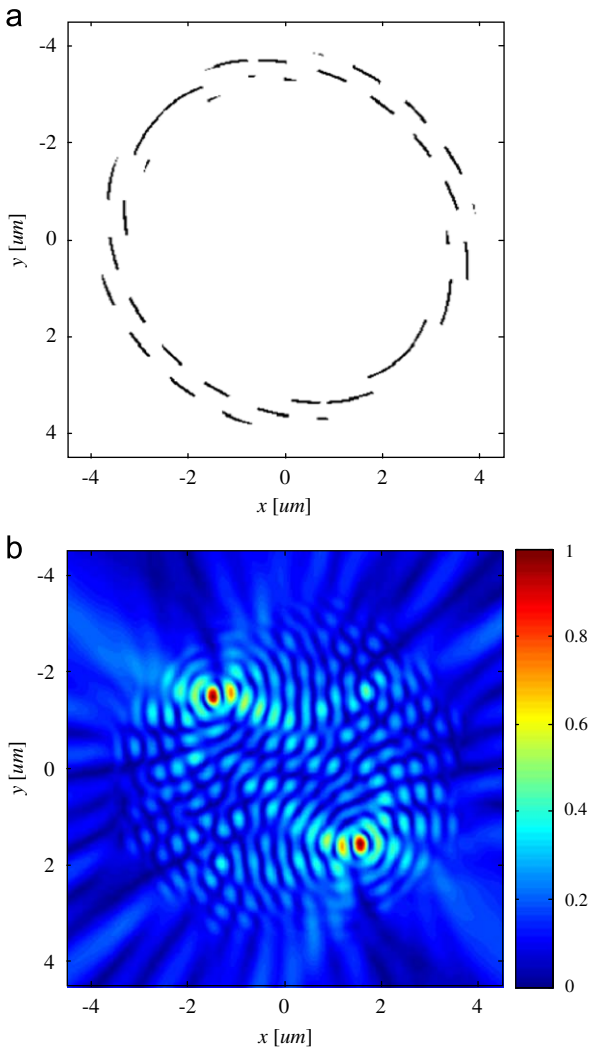

Fig. 26. (a) Diffractive slit patterns and (b) expected |**E**| for dual plasmonic focal spots based on a scalar model.

feature properly, these SPPs can be manipulated to generate focal spots on the metal surface.

In order to accomplish this, we devised diffractive slit patterns based on diffractive optics concepts [53]. Fig. 26(a) shows an example of a diffractive slit pattern generating two SPP focal spots. Using a simple scalar optics model, it becomes possible to obtain a simulation result, as seen in Fig. 26(b), where it is shown that two separated SPP focal spots are generated at different positions. Here if a light with x-directional polarization is normally incident on the metallic slit pattern from the backside, then SPP hot spots appear on the front surface of the metal, as shown in Fig. 26(b).

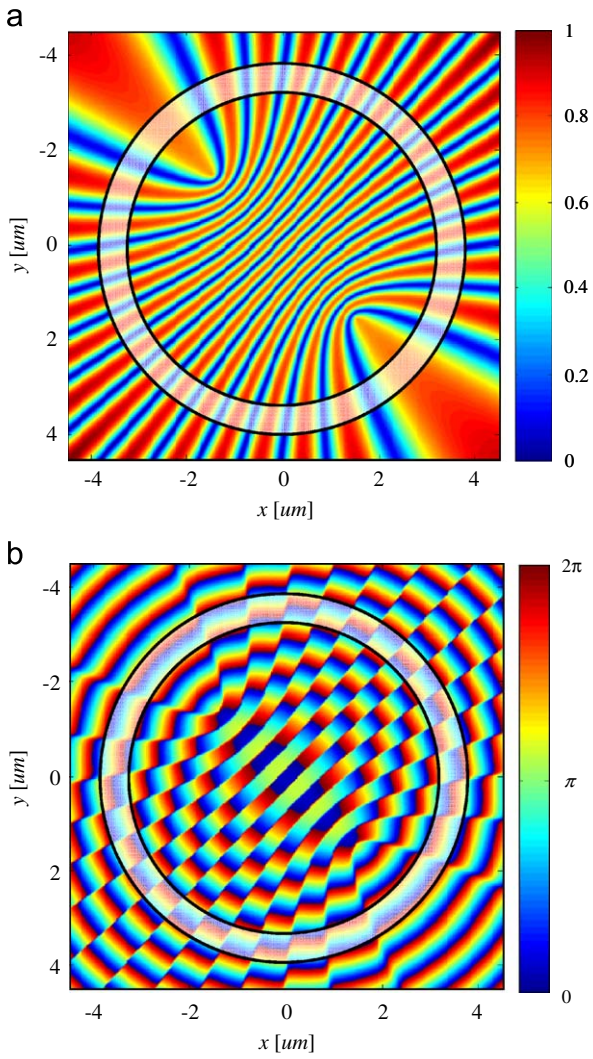

Fig. 27. (a) Amplitude distribution and (b) phase distribution of a composite field for two point sources centered at (1.5 μm, 1.5 μm) and (−1.5 μm, −1.5 μm).

Assuming that the slit pattern is pre-given as shown in Fig. 26(a), the SPP interference pattern of the simple scalar model, $U(x, y)$, is represented by

$$U(x,y) = \int_C \exp\left(jk_{SPP}\sqrt{(x-x')^2 + (y-y')^2}\right)\mathbf{p}\cdot\mathbf{n}\,ds, \tag{10}$$

where the slit curve is denoted by C with (x', y') coordinates, $\mathbf{p}$ and $\mathbf{n}$ are the polarization vector of the illuminating plane wave and the outer normal vector of the slit curve C, and ds is the differential length along the slit curve C. For the slit pattern shown in Fig. 26(a), the resulting SPP field distribution is obtained as shown in Fig. 26(b).

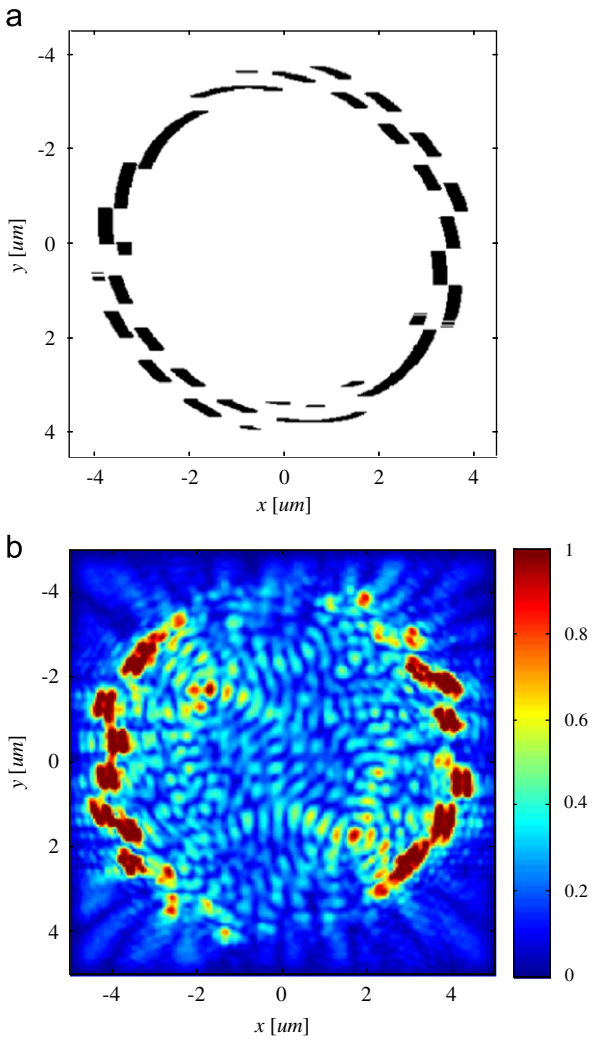

Fig. 28. (a) Diffractive slit patterns and (b) three-dimension RCWA simulation results for dual plasmonic focal spots.

Inversely, to design this slit pattern generating two separate SPP focal spots, we assume that the two point SPP sources are placed at specific positions and extract the equi-phase contours from the superposed field distribution of the point sources. Intuitively, by the Huygens principle, if continuously connected point sources with the same phase are placed on the equi-phase contour line, then the focal spots of the superposed SPP field distribution would likely appear at the same positions, which are the point source positions used to extract the equi-phase contour lines. This design concept is closely related to the methodology developed in the areas of holography and diffractive optics. In holography and diffractive optics, the phase profile of the optical field is recorded in the form of refractive index modulation inside the holographic media, diffractive optical elements or

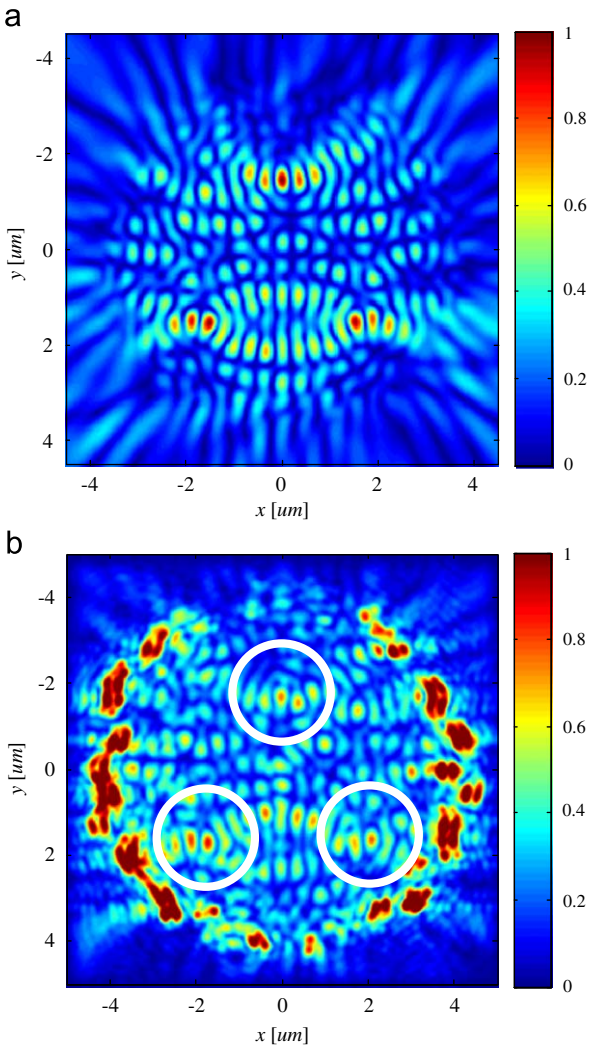

Fig. 29. (a) Scalar model and (b) full-vectorial simulation result of triple plasmonic focal spots.

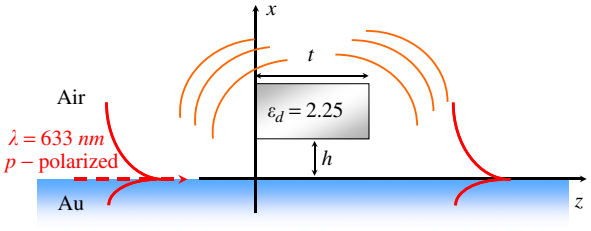

Fig. 30. Scattering feature of SPP in the floating dielectric block structure.

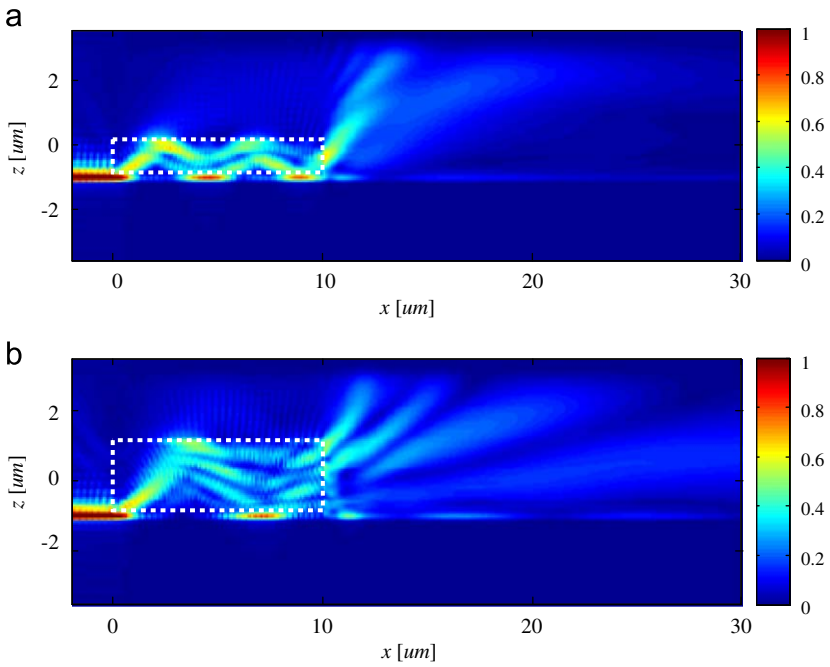

Fig. 31. |**E**| in the case of an air-gap thickness of 150 nm when the thickness of dielectric block ($\varepsilon_d = 2.25$) is (a) 1 μm and (b) 2 μm.

phase modulation devices such as liquid crystal spatial light modulators. In the design of diffractive slit patterns for SPP focusing, the same approach is used to record the phase profile of the signal field in the form of diffractive slit patterns.

Mathematically, the composite SPP signal field has the form of collectively summed circular wave components:

$$G(x,y) = \sum_m \exp\left(-jk_{spp}\sqrt{(x-x_m)^2 + (y-y_m)^2}\right) = a(x,y)\exp[j\phi(x,y)], \tag{11}$$

where $a(x, y)$ and $\phi(x, y)$ are the amplitude and phase functions of the composite optical field $G(x, y)$. Here $G(x, y)$ is composed of the circular wave components with the counter-directional wavenumber—k_{SPP}, which are diverging from the spot positions (x_m, y_m).

The diffractive slit pattern is simply formed on the equi-phase contour of the composite SPP signal field of Eq. (11). Fig. 27(a) and (b) show the amplitude and phase distributions of the composite field. We set a dim white band with outer and inner radii of R_1 and R_2 in each distribution. The equi-phase contour lines within the two rings are represented by Ω:

$$\Omega = \left\{(x,y)|\phi(x,y) = 0 \text{ and } R_2 \le \sqrt{x^2+y^2} \le R_1\right\}. \tag{12}$$

If a sub-wavelength curved slit pattern is formed following the path Ω in a thin metal film placed on the x–y plane ($z = 0$) and an x-directional polarization plane wave is normally incident on the backside of the metal film, SPPs excited on the front surface of

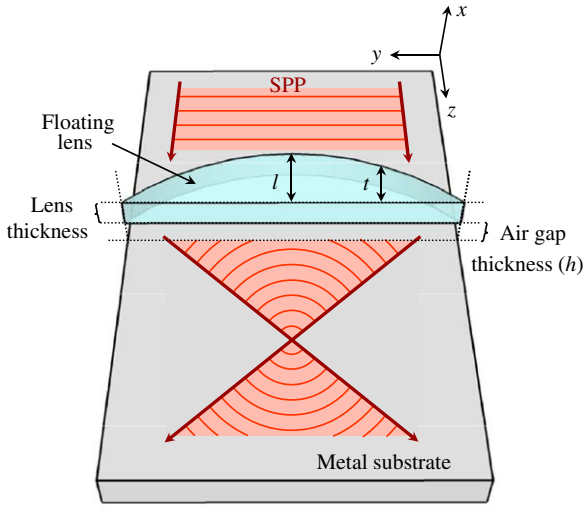

Fig. 32. Schematic of a floating dielectric lens for focusing an SPP.

the metal film by the curved slit propagate and produce complex interference patterns on the metal surface. In fact, in designing diffractive slit patterns for linearly-polarized incident optical fields, the polarity of SPP excitation should be carefully considered. This polarity problem is discussed in more detail in Ref. [53].

Fig. 28(a) and (b) show the diffractive slit patterns with finite sub-wavelength width sculptured along the equi-phase paths and three-dimensional RCWA simulation results for the diffractive slit pattern, respectively. In the simulation, x-directional polarization light having the wavelength of 633 nm is used, and the metal is Au. As proved in Fig. 28(b), the expectation of a scalar model is in good agreement with the simulation results.

Fig. 29 presents an example of resulting SPP field distributions generated by the diffractive slit patterns. To be specific, it shows three simultaneously formed SPP focal spot patterns.

5.2. *Surface plasmon focusing by using floating dielectric lenses*

There is a different feasible approaches for making the SPP focus on a metal surface by modulating the SPP fields using external dielectric media [54], as shown schematically in Fig. 30. The SPP eigenmode propagating on a metal surface is affected sensitively to the changes in the external refractive index. The artificial refractive index can be changed by simply floating a dielectric block near the metallic surface where the SPP is launched. When the dielectric block perturbs the SPP evanescent field, complex scattering occurs. When SPPs are launched on Au substrate by a light having the wavelength of 633 nm, Fig. 31(a) and (b) present scattering fields of SPPs passing through slightly floating dielectric blocks with different thicknesses of 1 and 2 μm, respectively.

A useful property of an SPP field inside this scattering phenomenon is phase modulation of the transmitted SPP field. The phase modulation is dependent on several structural factors such as dielectric block length, thickness, and its refractive index. An interesting

point is that it is possible to dynamically modulate the phase of SPP field with a fixed thickness dielectric block by adjusting the air gap within 50 nm [54]. This property cannot be found in bulk optics, in which the phase of incident optical fields can only be controlled by changing the thickness of the dielectric blocks.

Fig. 32 shows a dielectric lens for focusing an SPP field, which is a feasible application of the above-mentioned phase modulation property of SPP fields with a floating dielectric block. In Fig. 33(a) and (c), variations of the focal length of a parabolic and a Fresnel lens with a designed focal length of 12 μm for changing air-gap thickness are presented. In Fig. 33(b) and (d), variations in the focal length of parabolic and Fresnel lenses with a designed focal length of 8 μm for changing the air-gap thickness are shown. A linear change in the air-gap thickness, decreasing from 50 to 0 nm, gives a linear decrease in focal length to half the original focal length in the case of the floating parabolic lens, while a change in focal length is not observed in the case of the floating Fresnel lens. The Fresnel lens is less influenced by changes in air-gap since the focal length is mainly determined by the spatially fixed diffractive phase profile. Thus, it is possible to obtain a dynamic variable-focusing property using only the parabolic lens structure.

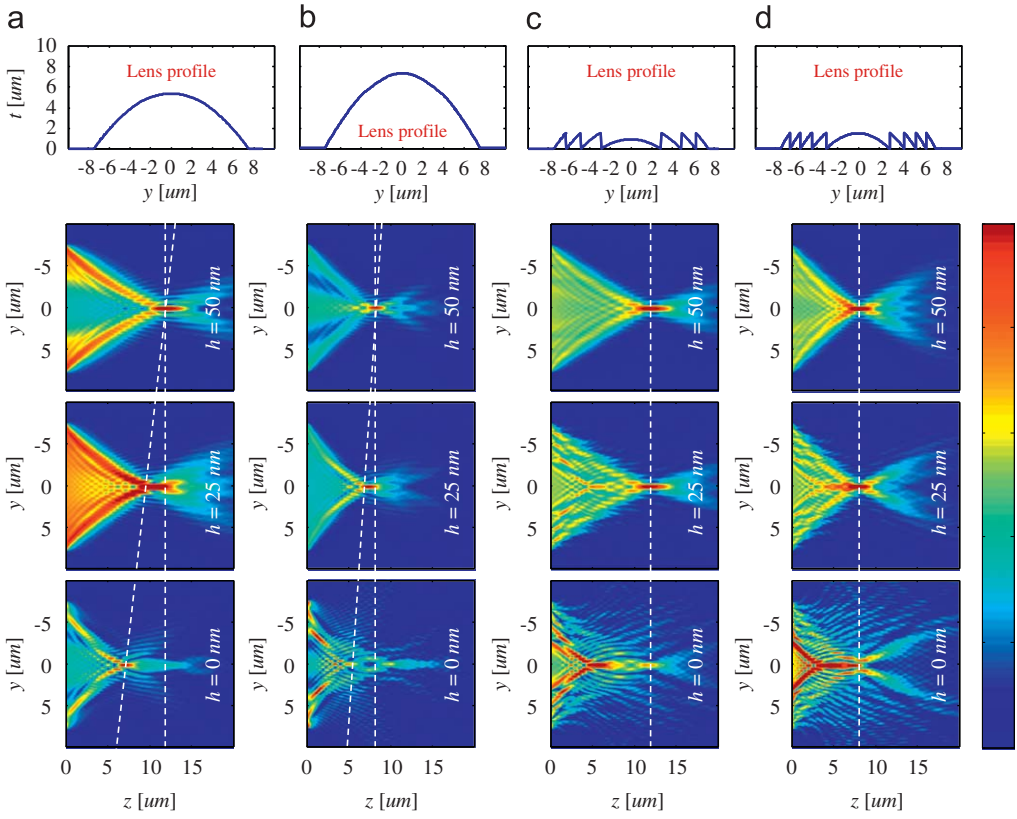

Fig. 33. Plasmonic focusing using a floating parabolic lens with a focal length of (a) 12 μm and (b) 8 μm as changing air gap thickness (h). Plasmonic focusing using floating Fresnel lens with a focal length of (c) 12 μm and (d) 8 μm as changing air gap thickness (h).

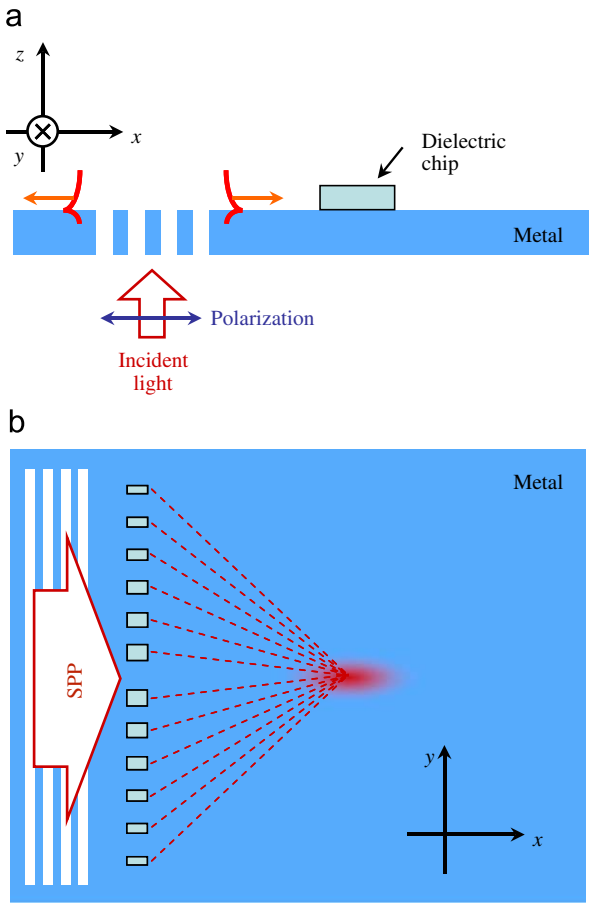

Fig. 34. (a) Lateral view and (b) top view of a plasmonic focusing structure using a dielectric Fresnel zone plate.

5.3. *Other methods to focus surface plasmon polaritons*

Some other methods are available for focusing light on a metal surface, and these methods are discussed in this Section. In particular, we will concentrate on three representative models in this plasmonic focusing field. Briefly, the first method for focusing an SPP is to use a dielectric Fresnel zone plate [55,56], and the second method is to utilize curvilinear sources such as perforated holes or an SPP condenser [57,58]. Lastly, the third method is to create a curved slit on the metal surface [59–63].

The use of the dielectric Fresnel zone plate is fundamentally similar to its use in beam focusing, and the basic scheme for such a structure is shown in Fig. 34 [55,56]. The basic principle is the same as that of a free space Fresnel zone plate in that the Fresnel zone plate plays a role in modulating the phase of the propagating SPP. In this manner, we can verify that SPPs also behave similarly to free-space light when they interact with Fourier based diffractive elements.

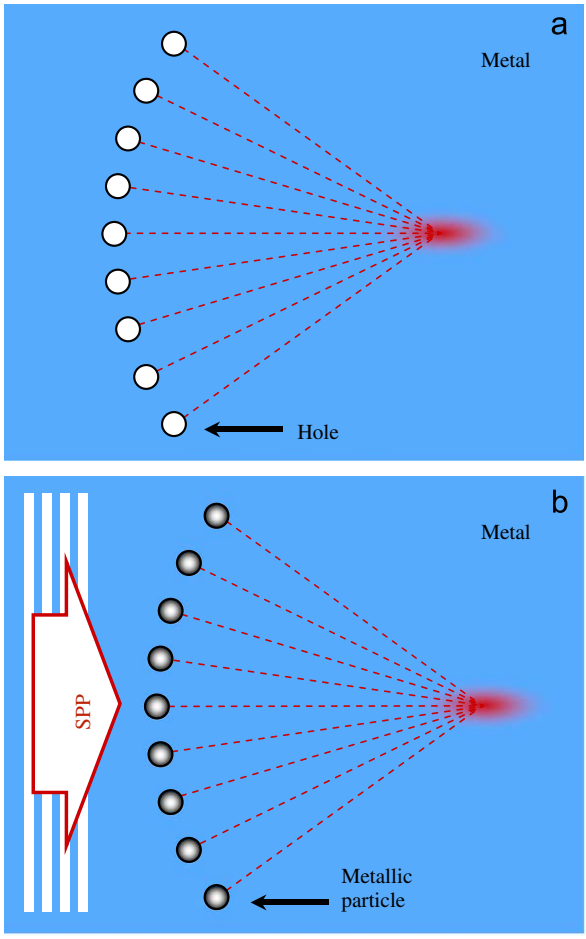

Fig. 35. Top view of a plasmonic focusing structure using (a) perforated holes and (b) SPP condensers.

If holes or SPP condensers are arranged in a curved shape, the SPPs come into focus [57,58]. Fig. 35(a) shows how to focus SPPs using perforated holes. In the first place, the light is impinged by back illumination, and then couples into holes as SPPs are generated. After the SPPs pass through these holes, they have concaved phase fronts due to the curved arrangement of the holes. As a result, they end up generating a plasmonic hot spot at some distance. In a similar way, metallic particles, or an SPP condenser, can be utilized, as shown in Fig. 35(b). In this case, when SPPs propagating on the metal surface meet curvilinear metallic particles, these metal particles act as virtual radiating elements. Consequently, SPPs modulated by metallic particles have concaved phase fronts, and the light is focused on the metal surface. Especially, it has been experimentally shown that this structure can be exploited in plasmonic waveguide coupler [57].

Fig. 36 shows our finite-difference time-domain (FDTD) simulation result for the case of Fig. 35(a). The substrate is Au and input light has a wavelength of 633 nm. Each hole has a

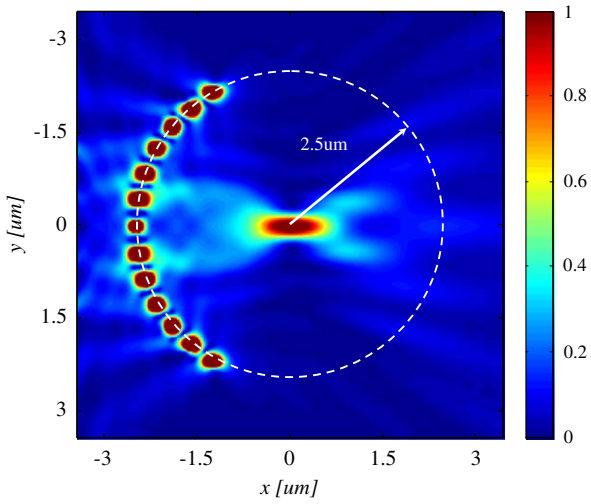

Fig. 36. FDTD simulation result of plasmonic focusing in case of structure using perforated hole array.

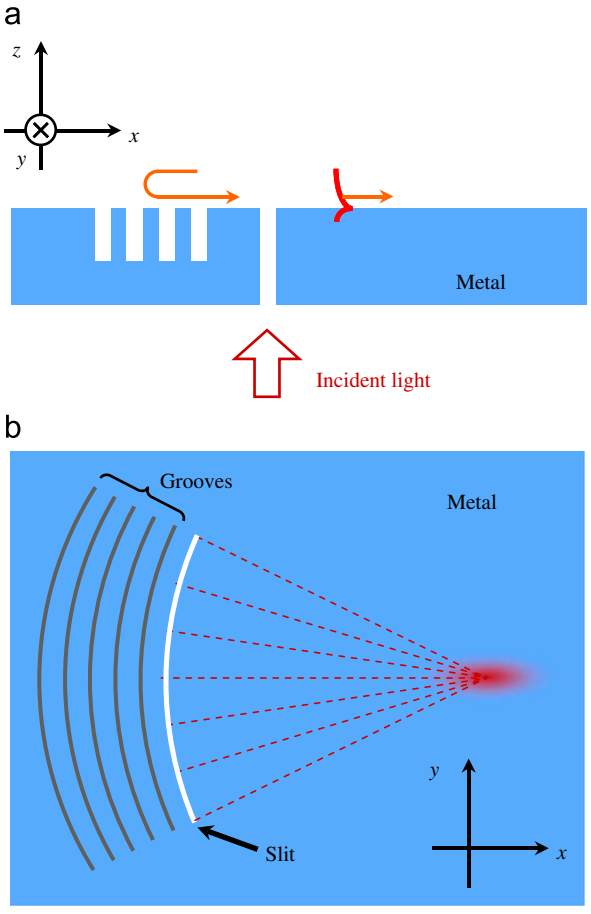

Fig. 37. (a) Lateral view and (b) top view of an enhanced plasmonic focusing structure using metallic grooves.

radius of 100 nm, and these holes are located on a white dashed circle having a radius of 2.5 μm.

Finally, the curved slit can be utilized in order to focus SPPs, and its basic principle is also based on modulating the phase front of the SPP [59]. After the SPPs pass through a curved slit, it is manifest that they become focused due to their modulated phase. There is an intriguing feature in this method. When metallic grooves are carved behind the slit, they act as Bragg gratings [60]. This indicates that SPPs propagating backward are reflected, and are able to contribute to the generation of a higher focal spot on the metal surface, as shown in Fig. 37.

In addition, it has been experimentally shown that the position of focal spot can be modified by impinging oblique light on curved slit structure [61–63]. As shown in Fig. 38(a), it is obvious that the plasmonic focal spot is formed at the center when radially polarized perpendicularly incident light is used in this plasmonic lens because all SPPs excited from circular slit are directed to the center of the plasmonic lens due to their symmetric phase. However, if the incident beam is inclined obliquely, there will be additional phase shift called the in-plane wave vector component of k_{in}, as shown in Fig. 38(b), and this additional component will adjust the direction of the excited SPPs. Therefore, the plasmonic focal center is shifted depending on this in-plane wave vector component, and the relation between the plasmonic focal spot displacement x and in-plane wave vector component k_{in} is given by

$$x^2\left(\frac{k_{spp}^2}{k_{in}^2}-1\right)=R^2-2Rx\cos\alpha, \tag{13}$$

where parameters R and α can be found in Fig. 38(b).

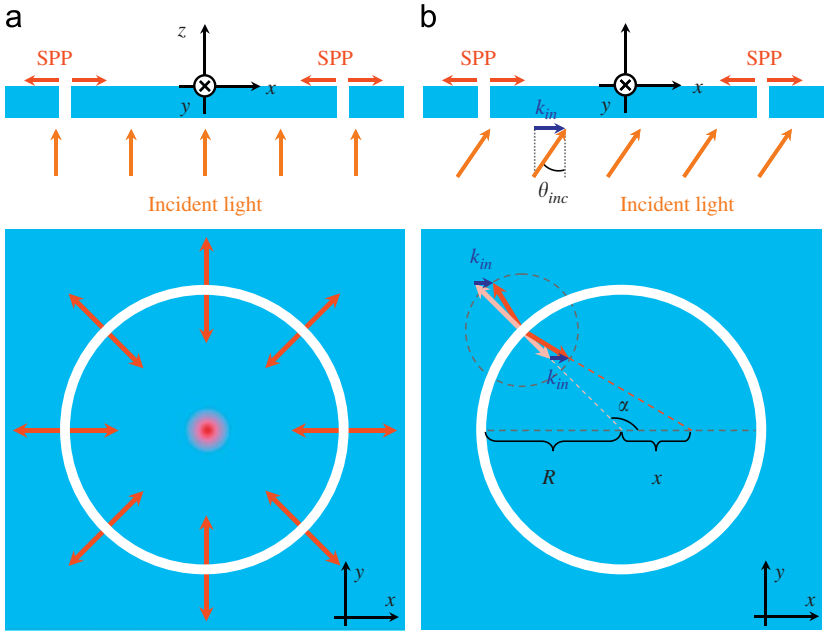

Fig. 38. The basic scheme for a plasmonic lens under (a) perpendicular and (b) obliquely incident light.

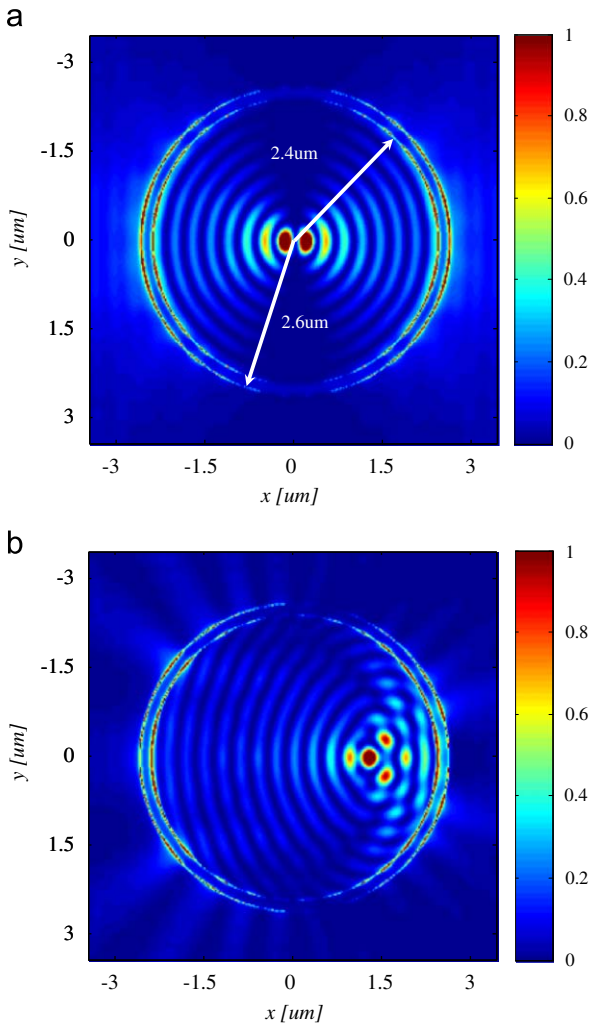

Fig. 39. FDTD simulation result of plasmonic lens when the incident angle of light is (a) 0° and (b) 30°.

Fig. 39 shows our FDTD simulation results as varying the incident angle of light. The substrate is Au, and the circular slit has a radius of 2.5 μm and a width of 200 nm. Fig. 39(a) shows a result when being impinged with a perpendicular incident light. As we expected, the focal spot is formed at the center of circular slit. Also, the shifting property depending on incident angle of input light is shown in Fig. 39(b) when the incident angle of light is 30°. From Eq. (13), it can be derived that focal spot is shifted by about 1.02 μm, and simulation result shows the focal spot is shifted by about 1.2 μm, reasonably.

Using this shifting property based on the incident angle of light, it has been reported that such shifted plasmonic focal spots can be used to multiplex SPPs on nano-wires [62]. To be specific, by changing the incident angle of light and controlling the displacement of the

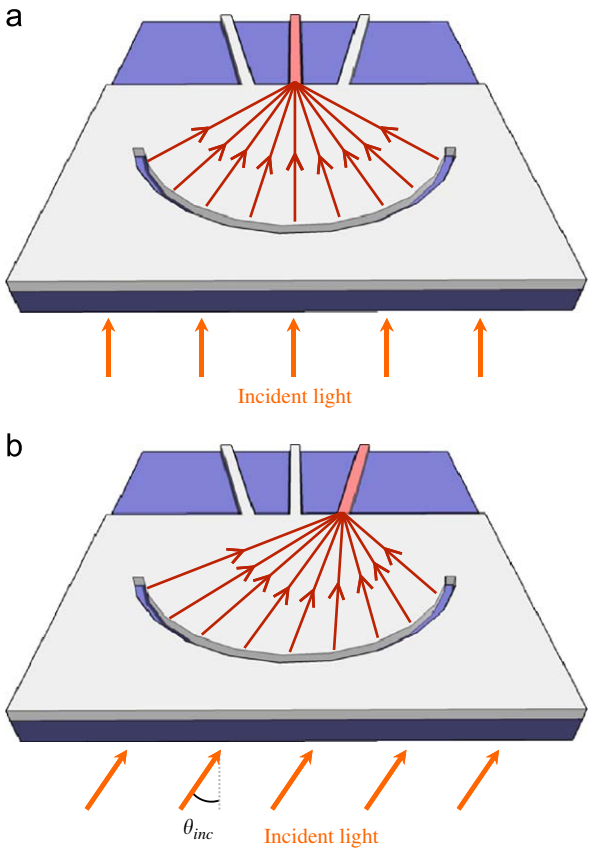

Fig. 40. Sketch of multiplexing surface plasmon polaritons on a nano-wire with (a) perpendicularly incident light and (b) obliquely incident light.

plasmonic focal spot, the coupling of SPPs into different nano-wire waveguides can be realized as shown in Fig. 40. Fig. 41 shows RCWA simulation results for the arc-shaped slit with perpendicular and oblique incident light.

In these slit structures of adopting slanted input light illumination, a careful design is needed because the SPP generation efficiency depends on the incidence angle and slit width [64].

6. Conclusion

In this paper, we discussed methods for controlling SPPs for generating spatially collimated or focused beams and plasmonic focal spots. Indeed, these methods of shaping light beams or SPPs are basically based on phase modulation. In manipulating spatial beams, surface gratings attached to a metal surface or sub-wavelength metal slit array play crucial roles in modulating the beam profiles. Also, the characteristics of focal spot and its position can be determined by diffractive slit patterns or diffractive elements controlling the phase of the SPPs. It would be expected that manipulating SPPs would contribute to further growth in nano-scale physics and engineering. Applications will be found in chip-

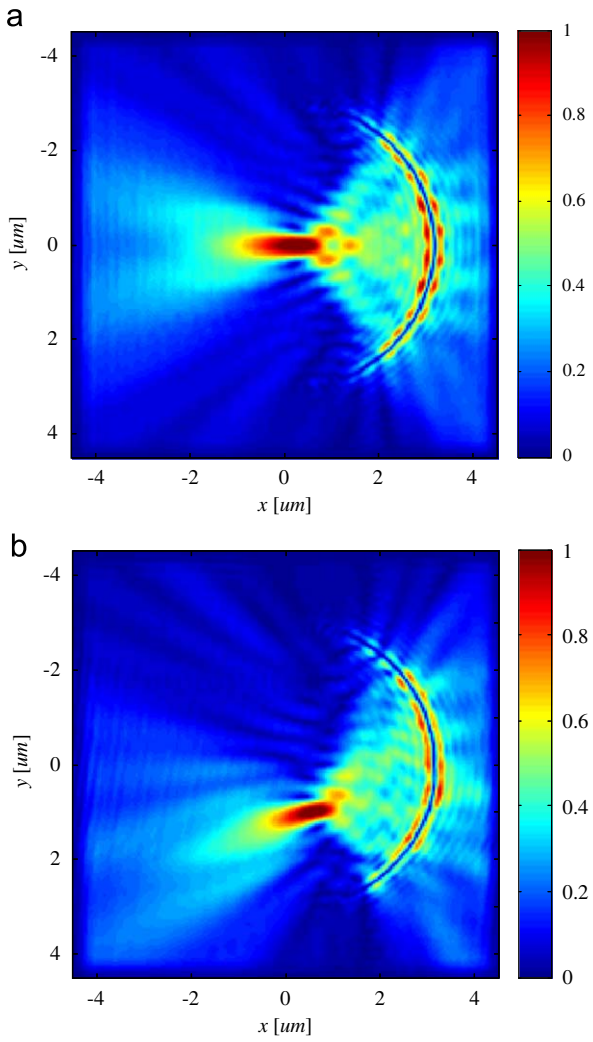

Fig. 41. RCWA simulation results: field distributions of focused SPPs with (a) perpendicular and (b) oblique incident light. The wavelength of light is 633 nm, and the substrate is composed of Au.

to-chip optical interconnections, optical data storage devices, optical detection, surface plasmon resonance sensing, etc. [65,66]. Further optimization of the structural design of those devices using the genetic algorithm [67] might be an important task.

Acknowledgments

This work was supported by the Ministry of Education, Science and Technology of Korea and Korea Science and Engineering Foundation through the Creative Research Initiatives Program (Active Plasmonics Application Systems).

References

[1] W.L. Barnes, A. Dereux, T.W. Ebbesen, Nature 424 (2003) 824–830.
[2] J. Takahara, S. Yamagishi, H. Taki, A. Morimoto, T. Kobayashi, Opt. Lett. 22 (1997) 475–477.
[3] W. Srituravanich, N. Fang, C. Sun, Q. Luo, X. Zhang, Nano Lett. 4 (2004) 1085–1088.
[4] Z.-W. Liu, Q.-H. Wei, X. Zhang, Nano Lett. 5 (2005) 957–961.
[5] N. Fang, H. Lee, C. Sun, X. Zhang, Science 308 (2007) 534–537.
[6] Z. Liu, H. Lee, Y. Xiong, C. Sun, X. Zhang, Science 315 (2007) 1686.
[7] K. Goto, Y. Kim, S. Mitsugi, K. Suzuki, K. Kurihara, T. Horibe, Jpn. J. Appl. Phys. 41 (2002) 4835–4840.
[8] K. Sendur, W. Challener, C. Peng, J. Appl. Phys. 96 (2004) 2743–2752.
[9] C.H. Gan, G. Gbur, Opt. Express 14 (2006) 2385–2397.
[10] T.W. Ebbesen, H.J. Lezec, H.F. Ghaemi, T. Thio, P.A. Wolff, Nature 391 (1998) 667–669.
[11] J.A. Porto, F.J. Garcia-Vidal, J.B. Pendry, Phys. Rev. Lett. 83 (1999) 2845–2848.
[12] L. Martin-Moreno, F.J. Garcia-Vidal, H.J. Lezec, K.M. Pellerin, T. Thio, J.B. Pendry, T.W. Ebbesen, Phys. Rev. Lett. 86 (2001) 1114–1117.
[13] C. Genet, T.W. Ebbesen, Nature 445 (2007) 39–46.
[14] H.J. Lezec, A. Degiron, E. Devaux, R.A. Linke, L. Martin-Moreno, F.J. Garcia-Vidal, T.W. Ebbesen, Science 297 (2002) 820–822.
[15] F.J. Garcia-Vidal, H.J. Lezec, T.W. Ebbesen, L. Martin-Moreno, Phys. Rev. Lett. 90 (2003) 213901.
[16] T. Thio, K.M. Pellerin, R.A. Linke, H.J. Lezec, T.W. Ebbesen, Opt. Lett. 26 (2001) 1972–1974.
[17] A. Agrawal, H. Cao, A. Nahata, New. J. Phys. 7 (2005) 249.
[18] H. Raether, Surface Plasmons on Smooth and Rough Surfaces and on Gratings, Springer-Verlag, Berlin, 1988.
[19] M. Dragoman, D. Dragoman, Prog. Quantum Electron. 32 (2008) 1–41.
[20] An.V. Zayats, I.I. Smolyaninov, J. Opt. A: Pure Appl. Opt. 5 (2003) S16–S50.
[21] S.A. Maier, Plasmonics: Fundamentals and Applications, Springer, United Kingdom, 2007.
[22] Y.A. Illinskii, L.V. Keldysh, Electromagnetic Response of Material Media, Plenum Press, New York, 1994.
[23] M.O. Marder, Condensed Matter Physics, John Wiley & Sons, Inc, New York, 2000.
[24] M.G. Moharam, E.B. Grann, D.A. Pommet, J. Opt. Soc. Am. A 12 (1995) 1068–1076.
[25] M.G. Moharam, D.A. Pommet, E.B. Grann, J. Opt. Soc. Am. A 12 (1995) 1077–1086.
[26] P. Lalanne, G.M. Morris, J. Opt. Soc. Am. A (1996) 779–784.
[27] P. Lalanne, E. Silberstein, Opt. Lett. 25 (2000) 1092–1094.
[28] H. Kim, I.-M. Lee, B. Lee, J. Opt. Soc. Am. A 24 (2007) 2313–2327.
[29] H. Kim, B. Lee, J. Opt. Soc. Am. A 25 (2008) 40–54.
[30] H. Kim, B. Lee, J. Opt. Soc. Am. B 25 (2008) 518–544.
[31] L. Martin-Moreno, F.J. Garcia-Vidal, H.J. Lezec, A. Degiron, T.W. Ebbesen, Phys. Rev. Lett. 90 (2003) 167401.
[32] L.B. Yu, D.Z. Lin, Y.C. Chen, Y.C. Chang, K.T. Huang, J.W. Liaw, J.T. Yeh, J.M. Liu, C.S. Yeh, C.-K. Lee, Phys. Rev. B 71 (2005) 041405.
[33] D.Z. Lin, C.K. Chang, Y.C. Chen, D.L. Yang, M.W. Liu, J.T. Yeh, J.H. Liu, C.H. Kuan, C.S. Yeh, C.K. Lee, Opt. Express 14 (2006) 3503–3511.
[34] S. Kim, H. Kim, Y. Lim, B. Lee, Appl. Phys. Lett. 90 (2007) 051113.
[35] H. Caglayan, I. Bulu, E. Ozbay, J. Phys. D: Appl. Phys. 42 (2009) 045105.
[36] N. Yu, J. Fan, Q.J. Wang, C. Pflugl, L. Diehl, T. Edamura, M. Yamanishi, H. Kan, F. Capasso, Nat. Photonics 2 (2008) 564–570.
[37] N. Yu, R. Blanchard, J. Fan, F. Capasso, T. Edamura, M. Yamanishi, H. Kan, Appl. Phys. Lett. 93 (2008) 181101.
[38] N. Yu, Q.J. Wang, C. Pflugl, L. Diehl, F. Capasso, T. Edamura, S. Furuta, M. Yamanishi, H. Kan, Appl. Phys. Lett. 94 (2009) 151101.
[39] T. Ishi, J. Fujikata, K. Makita, T. Baba, K. Ohashi, Jpn. J. Appl. Phys. 44 (2005) L364–L366.
[40] E. Laux, C. Genet, T. Skauli, T.W. Ebbesen, Nat. Photon 2 (2008) 161–164.
[41] P. Kramper, M. Agio, C.M. Soukoulis, A. Birner, F. Muller, R.B. Wehrspohn, U. Gosele, V. Sandoghdar, Phys. Rev. Lett. 92 (2004) 113903.
[42] E. Moreno, F.J. Garcia-Vidal, L. Martin-Moreno, Phys. Rev. B 69 (2004) 121402.
[43] I. Bulu, H. Caglayan, E. Ozbay, Opt. Lett. 30 (2005) 3078–3080.

[44] S.K. Morrison, Y.S. Kivshar, Appl. Phys. Lett. 86 (2005) 081110.
[45] K. Guven, E. Ozbey, Opt. Express 15 (2007) 14973–14978.
[46] H. Chen, X. Chen, J. Wang, W. Lu, Physica B 403 (2008) 4301–4304.
[47] S. Kim, Y. Lim, H. Kim, J. Park, B. Lee, Appl. Phys. Lett. 92 (2008) 013103.
[48] H. Shi, C. Wang, C. Du, X. Luo, X. Dong, H. Gao, Opt. Express 13 (2005) 6815–6820.
[49] C. Min, P. Wang, X. Jiao, Y. Deng, H. Ming, Appl. Phys. B 90 (2008) 97–99.
[50] H. Shi, C. Du, X. Luo, Appl. Phys. Lett. 91 (2007) 093111.
[51] Y. Fu, W. Zhou, L.E.N. Lim, Appl. Phys. Lett. 91 (2007) 061124.
[52] R.G. Mote, S.F. Yu, B.K. Ng, W. Zhou, S.P. Lau, Opt. Express 16 (2008) 9554–9564.
[53] H. Kim, B. Lee, Opt. Express 16 (2008) 8969–8980.
[54] H. Kim, J. Hahn, B. Lee, Opt. Express 16 (2008) 3049–3057.
[55] L. Feng, K.A. Tetz, B. Slutsky, V. Lomakin, Y. Fainman, Appl. Phys. Lett. 91 (2007) 081101.
[56] Q. Wang, X. Yuan, P. Tan, D. Zhang, Opt. Express 16 (2008) 19271–19276.
[57] L. Yin, V.K. Vlasko-Vlasov, J. Pearson, J.M. Hiller, J. Hua, U. Welp, D.E. Brown, C.W. Kimball, Nano Lett. 5 (2005) 1399–1402.
[58] W. Nomura, M. Ohtsub, T. Yatsui, Appl. Phys. Lett. 86 (2005) 181108.
[59] Z. Liu, J.M. Steele, W. Srituravanich, Y. Pikus, C. Sun, X. Zhang, Nano Lett. 5 (2005) 1726–1729.
[60] F. Lopez-Tejeira, S.G. Rodrigo, L. Martin-Moreno, F.J. Garcia-Vidal, E. Devaux, T.W. Ebbesen, J.R. Krenn, I.P. Radko, S.I. Bozhevolnyi, M.U. Gonzalez, J.C. Weeber, A. Dereux, Nat. Phys. 3 (2007) 324–328.
[61] Z. Liu, J.M. Steele, H. Lee, X. Zhang, Appl. Phys. Lett. 88 (2006) 171108.
[62] A. Imre, V.K. Vlasko-Vlasov, J. Pearson, J.M. Hiller, U. Welp, Appl. Phys. Lett. 91 (2007) 083115.
[63] H. Caglayan, I. Bulu, E. Ozbay, J. Appl. Phys. 130 (2008) 053105.
[64] H. Kim, B. Lee, Plasmonics 4 (2009) 153–159.
[65] W.A. Challener, C. Peng, A.V. Itagi, D. Karns, W. Peng, Y. Peng, X.M. Yang, X. Zhu, N.J. Gokemeijer, Y.-T. Hsia, G. Ju, R.E. Rottmayer, M.A. Seigler, E.C. Gage, Nat. Photon 3 (2009) 220–224.
[66] B. Lee, S. Roh, J. Park, Opt. Fiber Technol. 15 (2009) 209–221.
[67] J. Jung, M. Kim, J. Opt. Soc. Korea 11 (2007) 55–58.